



Evaluation of the anisotropic grain boundaries and surfaces of alpha U via molecular dynamics

May 2024

Changing the World's Energy Future

Khadija Mahbuba, Benjamin W Beeler, Andrea M Jokisaari



DISCLAIMER

This information was prepared as an account of work sponsored by an agency of the U.S. Government. Neither the U.S. Government nor any agency thereof, nor any of their employees, makes any warranty, expressed or implied, or assumes any legal liability or responsibility for the accuracy, completeness, or usefulness, of any information, apparatus, product, or process disclosed, or represents that its use would not infringe privately owned rights. References herein to any specific commercial product, process, or service by trade name, trade mark, manufacturer, or otherwise, does not necessarily constitute or imply its endorsement, recommendation, or favoring by the U.S. Government or any agency thereof. The views and opinions of authors expressed herein do not necessarily state or reflect those of the U.S. Government or any agency thereof.

Evaluation of the anisotropic grain boundaries and surfaces of alpha U via molecular dynamics

Khadija Mahbuba, Benjamin W Beeler, Andrea M Jokisaari

May 2024

**Idaho National Laboratory
Idaho Falls, Idaho 83415**

<http://www.inl.gov>

**Prepared for the
U.S. Department of Energy
Under DOE Idaho Operations Office
Contract DE-AC07-05ID14517**

Evaluation of the anisotropic grain boundaries and surfaces of α -U via molecular dynamics

Khadija Mahbuba^a, Benjamin Beeler^{a,b}, Andrea Jokisaari^b

^a*North Carolina State University, Raleigh, NC 27607*

^b*Idaho National Laboratory, Idaho Falls, ID 83415*

Abstract

Alloys based on uranium-zirconium are gaining renewed interest as fuels for the Versatile Test Reactor and a number of microreactor designs. Implementing metallic fuel in reactors creates the need for robust descriptive and predictive fuel performance modeling. The current state of metallic fuel performance modeling relies on empirical equations derived from historical experiments, which may be unreliable when applied outside of their temperature, power, and composition phase space. One area where such data is lacking is the irradiation behavior of α -U, specifically tearing and porosity formation at the early stages of irradiation. While grain boundaries likely play a key role in this fuel behavior, relatively little is known about grain boundaries in α -U. Thus, we evaluate the grain boundary, surface energy, and work of adhesion of α -U utilizing molecular dynamics. Symmetric tilt grain boundaries (STGBs) are analyzed with the tilt plane oriented along each major crystallographic axis, for a total of eighty unique grain boundaries. The effect of temperature, tilt plane, and misorientation angle on interfacial energies are analyzed. The interfacial energies typically increase with temperature and there is significant variance as a function of misorientation angle, irrespective of the tilt plane. At 500 K, the average surface energy (1.23 J/m^2) is approximately 1.5 times the grain boundary energy (0.79 J/m^2), and the work of adhesion is approximately twice the grain boundary energy (1.68 J/m^2). Orientations for the likely formation of twins and likely failure planes are identified.

1. Introduction

Two life-limiting phenomena in metallic fuels are fission gas release and fuel-clad chemical interaction (FCCI) [1]. Both of these phenomena are affected by fuel swelling, which is driven by the development of porosity and fission gas bubbles. Fuel swelling in U-Zr metallic fuel is anisotropic and highly dependent upon the phase of U [2]. Within metallic fuel, it is expected that all three U allotropes are present due to both the temperature gradient across the fuel slug and the alloying composition. The low-temperature allotrope of U, α -U, is stable up to 935 K [3] and has a low symmetry orthorhombic structure with four atoms in the unit cell, as shown in Figure 1 [4].

The $(0\ 0\ 1)$ plane of α -U can be considered to be a distorted body-centered cubic (bcc) $(1\ 1\ 0)$ plane, where alternate parallel bcc $(1\ 1\ 0)$ planes are offset by a distance of $2y$ along the $\langle 0\ 1\ 0 \rangle$ axis, where y is

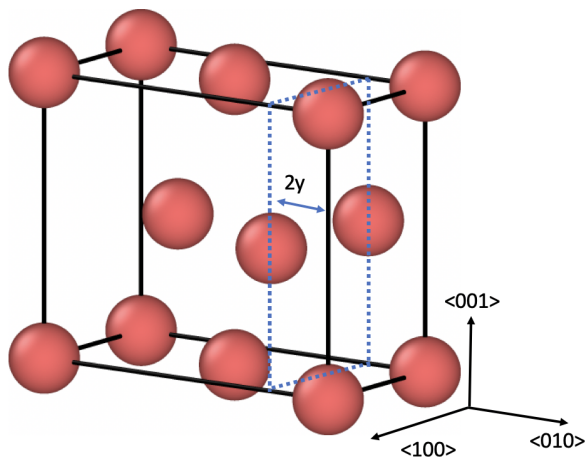


Figure 1: Orthorhombic α -U unit cell [4], which has mirror symmetry with respect to the (100) and (001) planes among the three major planes. The (0 1 0) plane is similar to the (1 1 0) plane of a bcc structure where alternate bcc (1 1 0) planes are offset by $2y$ distance

an internal coordinate [5]. This geometry has two mirror symmetries with respect to the (1 0 0) and (0 0 1) planes [6, 7, 8]. Because of its unique crystal structure, α -U exhibits anisotropic material properties, for example, thermal expansion [9] and elastic constants [10]. α -U has a negative thermal expansion coefficient in the $\langle 0 1 0 \rangle$ direction from 300 K to 923 K [9], which is probably the result of anisotropy and the temperature dependence of elastic properties. Furthermore, single-crystal α -U experiences irradiation-induced growth without a significant change in volume, in which a crystal macroscopically enlarges in the $\langle 0 1 0 \rangle$ direction and shrinks in the $\langle 1 0 0 \rangle$ direction [11]. The irradiation growth appears to be much larger at cryogenic temperatures than at 293 K, but its behavior at elevated temperatures (e.g., 700 K) is still unknown [11].

Polycrystalline α -U displays complex behavior due to the fundamental anisotropy of the crystal structure and the presence of internal microstructure [12]. Because grain boundaries (GBs) act as sinks for irradiation-induced point defects and also hinder dislocation movement, they are a very important feature affecting the deformation and plasticity of α -U. A common type of GB is a symmetric tilt grain boundary (STGB), which has a mirror symmetry across the tilt plane with some amount of atomic misfit. Twinning is a special STGB in which there is a minimal atomic misfit across the GB plane [13, 14], typically resulting in a very low grain boundary energy [15]. Generally, low symmetry materials, such as α -U, magnesium, and beryllium, deform via several distinct modes of dislocation slip and twinning, and the relative activation of these slip modes is sensitive to grain orientation and temperature [16, 17]. However, to the authors' knowledge, no work is available on the properties of STGBs in α -U, although some research has been performed on twinning.

The earliest experimental work on the deformation of α -U via twinning was conducted in the early 1950s [7, 8, 18, 19]. Through a detailed crystallographic analysis of deformation twinning, forty-one possible twins of α -U [20] were found. It has also been observed that twins possessing a low shear factor (less than 1) are the most prominent [8, 18, 7, 20].

The effect of grain boundaries on the swelling of polycrystalline α -U remains largely unknown. It has been observed that grain boundary tearing is responsible for 50% of the reported pure U swelling [21].
35 Cavitation swelling at low temperatures is related to the anisotropic growth of α -U and appears to be related to twinning [2], which we emphasize, is a special type of STGB. These cavities primarily form at grain boundaries and junctions, especially at twin boundaries and junctions [22]. Though twin boundaries are not a preferable nucleation site for recrystallization, the nucleation of recrystallized grains is highly correlated with high-angle grain boundary locations [23].

40 The energy cost to make a cavity along the grain boundary can be expressed as the energy required to break the bonds between two existing grains [24]. This energy is called the work of adhesion (WAd), or cleavage energy, and can be interpreted as the energy difference of a STGB versus two surfaces of the same orientation. Work of adhesion is important to know how much normal stress a grain boundary can withstand [25]. Thus, the surface energy is also required to evaluate the mechanical performance of α -U.
45 Experimental and computational studies report that the surface energy can vary from 0.5 J/m² to 2.5 J/m² [5, 26, 27, 28]. However, none of these studies were thorough in their surface orientation examinations. Most recently, density functional theory was used to calculate the surface energy of seven unique surfaces, and energies ranged from 1.756 J/m² to 2.151 J/m² [29]. This study examined a subset of potential surfaces and provides a qualitative sense of the magnitude of surface energies in α -U, but is far from a complete data set.

50 The ability to predict the microstructural evolution of α -U under irradiation and subjected to temperature gradients relies on an accurate understanding of interfacial properties, including GB and surface energies. Such energetic properties can serve to provide fundamental insight into the expected fission gas bubble behavior, interfacial orientations, GB mobility, and tearing. Molecular dynamics is a powerful tool to analyze the interfacial energy, given the availability of a suitable interatomic potential [24, 30]. The current
55 work performs a computational analysis to evaluate the GB energy and surface energy related to STGBs by molecular dynamics. Interfacial energies are determined as a function of temperature (300 K, 400 K, 500 K, and 600 K) and misorientation angle. Finally, using grain boundary energies and corresponding surface energies, the work of adhesion for different STGBs is evaluated.

2. Computational Details

60 The Large-scale Atomic/Molecular Massively Parallel Simulator (LAMMPS) [31] is utilized to perform molecular dynamics (MD) simulations. The authors have prepared the STGB geometry by two methods. In method 1, a simulation box is selected and divided into two regions to generate the supercell. Region one is tilted by $\theta/2$, without distorting the lattice of α -U, with respect to the defined tilt axis, where θ is the misorientation angle and the tilt axis is parallel to the tilt plane (or cut plane). Taking the reflection of the
65 former region across the tilt plane, region two is created, and, in the process, two symmetric tilt GBs are generated; one in the center of the supercell, and one across the periodic boundary normal to the tilt plane. To generate the surface, region two (or the mirrored region) of the supercell is considered a vacuum.

In method 2, the symmetrical grain boundary structure is generated in an identical way, except that each grain is generated such that it has a free surface. The system is then relaxed, allowing for surface reorientation, and then the system is brought into contact, generating a bi-crystal in the supercell. This can be considered identical to method 1, but with the added stage of surface relaxation. A subset of seven STGBs is utilized to compare the GB energy of respective STGBs generated with both methods. It has been observed that for some STGBs, method 1 predicts a lower GB energy, while for other STGBs method 2 predicts lower energies. However, the discrepancy between the two methods is limited to a maximum of 10%. Another method of calculating GB energy, which is not utilized in this work, is the γ surface method. The γ surface method is not employed, because above 0 K, atoms at GBs reorient to their relaxed orientation if sufficient relaxation time is provided, making this method less effective at higher temperatures [32]. Method 1 was chosen as the standard method of GB construction and equilibration, as negligible improvements were observed with an additional surface relaxation step.

The size of the supercell depends on the orientation of the STGB plane or surface investigated, which is selected such that the two-grain boundary planes or surfaces present within a single supercell are non-interacting while also satisfying periodic boundary conditions in all directions. Thus, the number of atoms varies by grain boundary geometry, ranging from 968 to 4,800 atoms. System sizes were observed to be converged with respect to interfacial energy. In this work, we utilize a STGB nomenclature of $(h\ k\ l)\langle p\ q\ r\rangle$, where $(h\ k\ l)$ is the misorientation plane and $\langle p\ q\ r\rangle$ is the tilt axis. A total of eighty STGBs were constructed: with twenty-four STGBs with tilt axis $\langle 1\ 0\ 0\rangle$ and shear plane $(0\ 0\ 1)$, twenty-four with tilt axis $\langle 0\ 0\ 1\rangle$ and shear plane $(0\ 1\ 0)$, and thirty-two with tilt axis $\langle 0\ 0\ 1\rangle$ and shear plane $(1\ 0\ 0)$, such that a broad scope of STGBs is investigated with respect to the three crystallographic primary shear planes. Grain boundaries (or surfaces) of $(h\ k\ 0)\langle 1\ 0\ 0\rangle$, $(h\ 0\ k)\langle 0\ 0\ 1\rangle$, and $(0\ h\ k)\langle 0\ 0\ 1\rangle$ series are named as type A, B, C, respectively, and shown in the Appendix (Figure 10). Grain boundaries and surfaces, along with their misorientation angle and tilt axis are listed in the Appendix (Table 1 and Table 2, respectively). Misorientation angles considered in the current work are classified into two domains: one is 0° to 180° , and another is 180° to 360° . All of the three investigated shear planes have a symmetry of 180° , so theoretically the trend of GB energy with misorientation angle should have mirror symmetry with respect to $(1\ 0\ 0)$, $(1\ 0\ 0)$, and $(0\ 0\ 1)$ planes in type A, B, and C STGBs, respectively. The reason behind the two domains is to validate the result with theory.

An as-constructed type A STGB plane $(\bar{1}\ 12\ 0)\langle 1\ 0\ 0\rangle$ is shown in Figure 2(a). In this Figure, $(0\ 1\ 0)$ is the tilt plane (or cut plane), the left hand side of the supercell is tilted 80.54° with respect to the $\langle 1\ 0\ 0\rangle$ tilt axis, and the right-hand side is the mirror of left-hand side. Here, tilting follows the right hand rule, where $(0\ 0\ 1)$ is the shear plane (parallel to the drawing surface) and the STGB is produced at the $(0\ 1\ 0)$ plane (perpendicular to the drawing surface). OVITO is utilized for visualization [33]. In a similar fashion, one example from type B STGB, $(\bar{2}\ 0\ 1)\langle 0\ 0\ 1\rangle$ and one from type C STGB, $(0\ 6\ \bar{5})\langle 0\ 0\ 1\rangle$ are presented in Figure 2(b) and (c), respectively.

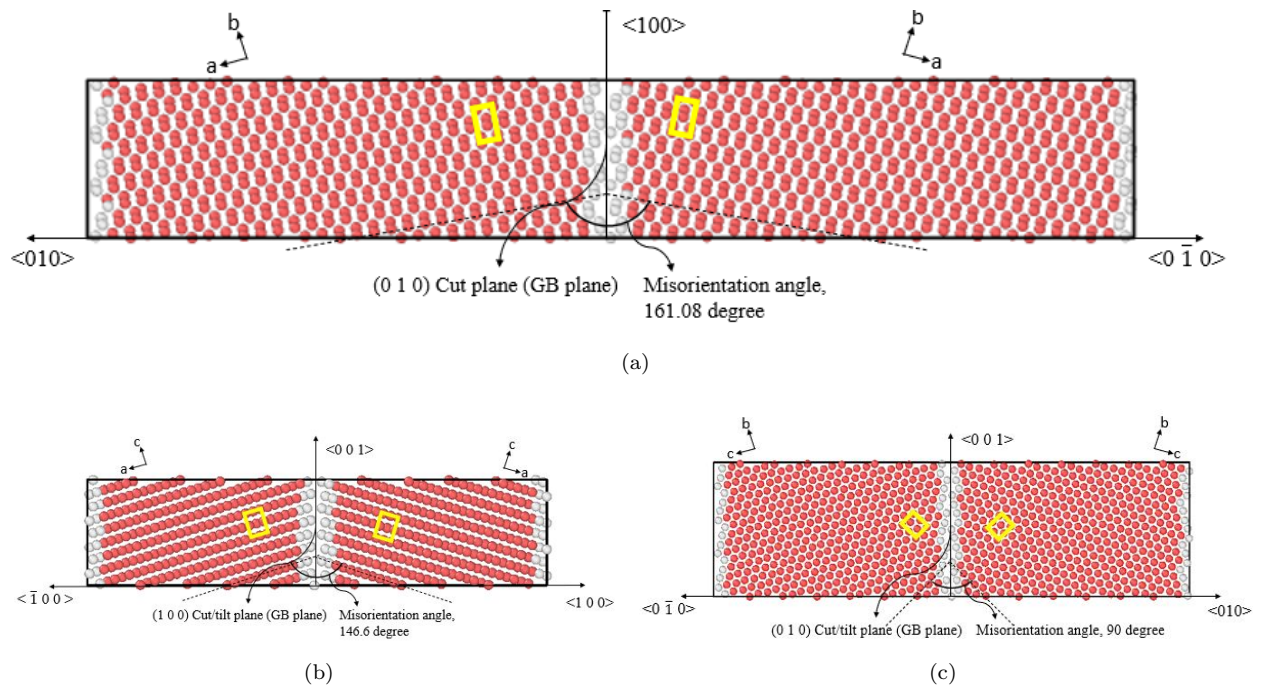


Figure 2: The as-constructed α -U symmetric tilt grain boundary (STGB) (a) $(\bar{1} 12 0)\langle 1 0 0 \rangle$ with respect to the $(0 1 0)$ tilt plane (or cut plane). Grain boundaries exist in the middle and on the edges of the super cell. Here the $(0 0 1)$ plane is the shear plane. Both red and white atoms are U, but with different coordination environments to illustrate grain boundaries. Yellow rectangles indicate the α -U unit cell and a, b, and c represent the original $\langle 1 0 0 \rangle$, $\langle 0 1 0 \rangle$, and $\langle 0 0 1 \rangle$ crystal structure orientation (i.e. the axis of the region). In a similar way (b) $(\bar{2} 0 1)\langle 0 0 1 \rangle$ and (c) $(0 6 \bar{5})\langle 0 0 1 \rangle$ STGBs are shown which has shear plane at the $(0 1 0)$ and the $(1 0 0)$ plane respectively.

For simplicity of construction of STGBs, the lattice parameters of α -U are considered as $a=3$, $b=6$, $c=5$ Å, instead of the equilibrium lattice parameters of $a=2.8$, $b=5.8$, $c=4.9$ at room temperature Å [4, 34]. However, sufficient relaxation of the system is performed to ensure equilibrated systems, with equilibrium lattice constants, for the analysis of stable grain boundaries. Due to the utilization of an NPT ensemble with periodic boundaries and the independent relaxation of each lattice vector, the imposed stresses from the simulation setup are rapidly relaxed. Individual unit cells from the grain interior were analyzed to ensure equilibrium lattice constants were present.

The UMo angular dependent potential (ADP) from Ref. [35] is used in this work. This interatomic potential reasonably predicts a number of properties in α -U, γ -U, and γ -UMo alloys. A Nose-Hoover barostat is considered for the anisotropic relaxation of the system in all directions with a damping factor of 0.1. For temperature control, a Langevin thermostat is utilized with a relaxation time of 0.1 ps. The system is observed at temperatures of 300 K, 400 K, 500 K, and 600 K, where U is present in the α phase. When the volume and energy of the system reach equilibrium, the values of observable parameters (energy and volume) are collected. Systems are equilibrated for 200 ps to 250 ps, and energies are averaged over the final 50 ps. To ensure statistical significance, each system is simulated three to five times, each with a unique initial distribution of velocities. This yields a maximum standard error of approximately 5% for interfacial energies.

The interfacial energies are calculated as

$$E_{\text{inf}} = \frac{E^* - E_0}{2A} \times N \quad (1)$$

where E_{inf} is the interfacial (STGB or surface) energy per unit interface (STGB or surface) area, E^* is the internal energy per atom of a system with an interface, N is the number of atoms in the system with an interface, E_0 is the internal energy per atom of a defect-free system, and A is the area of each interface (as there are two interfaces per supercell, there is $2A$ in the denominator). In addition, the work of adhesion of STGBs is calculated as

$$W_{\text{ad}} = 2 \times E_{\text{inf}(\text{surface})} - E_{\text{inf}(\text{STGB})} \quad (2)$$

where $E_{\text{inf}(\text{surface})}$ is the surface energy per unit area and $E_{\text{inf}(\text{STGB})}$ is the GB energy per unit area.

STGBs with very low energies (per the definition in Ref. [13]) will be considered as preferable twinning orientations, and the remaining STGBs will be considered general STGBs in the following sections. The definition of interfacial energy in equation 1 only considers the potential energy, while it is the GB free energy that will determine the true energetic behavior of GBs. While ΔS can be implicitly calculated from E_{inf} at different temperatures [36]. However, entropic effects would not affect the conclusions or qualitative relationships determined within this work. The temperatures are relatively low (below 600 K) and Beeler et al. [37] have shown at higher temperatures in similar metallic systems that the effect of entropy on grain boundary energies will be on the order of 10 mJ/m²-K, whereas the GB energy calculated in the current work is on the order of 1000 mJ/m². Thus, the effect of entropy can be reasonably neglected here.

3. Results and Discussions

3.1. Grain Boundary Energies

3.1.1. Effect of misorientation angle

140 The GB energy calculated for all eighty STGBs is plotted as a function of misorientation angle in Figure 3 at 500 K. Each type of STGB (A, B, and C) has been studied for misorientation angles from 0° to 360° . As per the methodology section, only STGBs with a misorientation angle of 0° to 180° are discussed in the following sections, and their mirror symmetries are verified and plotted. There is no data available in the literature that could be explicitly compared with the result of the current work. Data points are connected
145 by straight lines to guide the eye.

Type A STGBs ($\langle 1\ 0\ 0 \rangle$ tilt axis) have deep cusps at the $(0\ 1\ 0)$ (similar $(0\ \bar{1}\ 0)$ plane) and $(\bar{3}\ 12\ 0)$ plane, with corresponding GB energies of $0.36\ \text{J/m}^2$ and $0.27\ \text{J/m}^2$. At 0° and 360° , both regions (tilted and mirror of tilted) of the supercell have their major axis ($\langle 1\ 0\ 0 \rangle$ and $\langle 0\ 1\ 0 \rangle$) parallel to their respective axes of the supercell. As α -U does not have mirror symmetry with respect to the $(0\ 1\ 0)$ plane, a GB is
150 created at the junction of two regions, albeit with a small atomic misfit. Thus, the $(0\ 1\ 0)$ and $(0\ \bar{1}\ 0)$ orientations have a cusp in the GB energy profile. At the 180° misorientation, both sides (or regions) have their $\langle 0\ 1\ 0 \rangle$ axis parallel to the $\langle 1\ 0\ 0 \rangle$ axis of the supercell. Because of the symmetry of the $(1\ 0\ 0)$ plane of α -U, this orientation does not describe any GB and is instead the pure crystalline system, resulting in zero grain boundary energy. As seen in Figure 3(a), the highest GB energy is $0.9\ \text{J/m}^2$, which occurs at
155 the 14.25° misoriented STGB $(\bar{1}\bar{2}\ 3\ 0)\langle 1\ 0\ 0 \rangle$. The GB energy increases as the misorientation increases up to 15° , and decreases as misorientation increases to 180° , ignoring the cusp. The shape of the GB energy versus misorientation angle has a mirror symmetry with respect to the $(1\ 0\ 0)$ plane. Type A STGBs have an average grain boundary energy of $0.71\ \text{J/m}^2$, as obtained by simple averaging. Because the lowest GB energy among the type A STGB is the $(\bar{3}\ 12\ 0)\langle 1\ 0\ 0 \rangle$ orientation, it would be a likely candidate to form twins.
160 Without considering the major cusps (very low energy STGBs), the average GB energy of general STGBs is $0.78\ \text{J/m}^2$. It has been experimentally observed that in α -U, grains are always oriented in a direction that is more than 60° from the $\langle 1\ 0\ 0 \rangle$ direction (i.e. around the $\langle 0\ 1\ 0 \rangle$ direction) in pure α -U [38]. We show that STGBs tilted with respect to the $\langle 1\ 0\ 0 \rangle$ axis between 63.4° to 116.6° have very low energies ($0.23\ \text{J/m}^2$ to $0.72\ \text{J/m}^2$, which is equal or lower than the average GB energy compared to other STGBs of type A. This
165 seems to support the previous experimental findings.

The grain boundary energy of type B STGBs ($\langle 0\ 0\ 1 \rangle$ tilt axis) has a minor cusp at the $(\bar{2}\ 0\ 1)$ plane with a corresponding GB energy of $0.58\ \text{J/m}^2$. The highest GB energy for type B STGBs has been observed at the $(\bar{1}\ 0\ 4)\langle 0\ 0\ 1 \rangle$ with a value of $0.89\ \text{J/m}^2$. The GB energy of type B STGBs is maximal when grains are oriented between 20° to 40° angle tilted from the $\langle 0\ 0\ 1 \rangle$ axis. It should be noted that the maximum
170 planar density for $(h\ 0\ k)$ surfaces occurs at a tilt angle 31° (Figure 10 in the Appendix). At 0° , 180° , and 360° misorientations, the $\langle 0\ 0\ 1 \rangle$ axis of supercell is parallel to $\langle 1\ 0\ 0 \rangle$, $\langle 0\ 0\ 1 \rangle$, and $\langle 1\ 0\ 0 \rangle$ axis of both regions of supercell (crystal axis), respectively. These orientations do not create any grain boundaries due

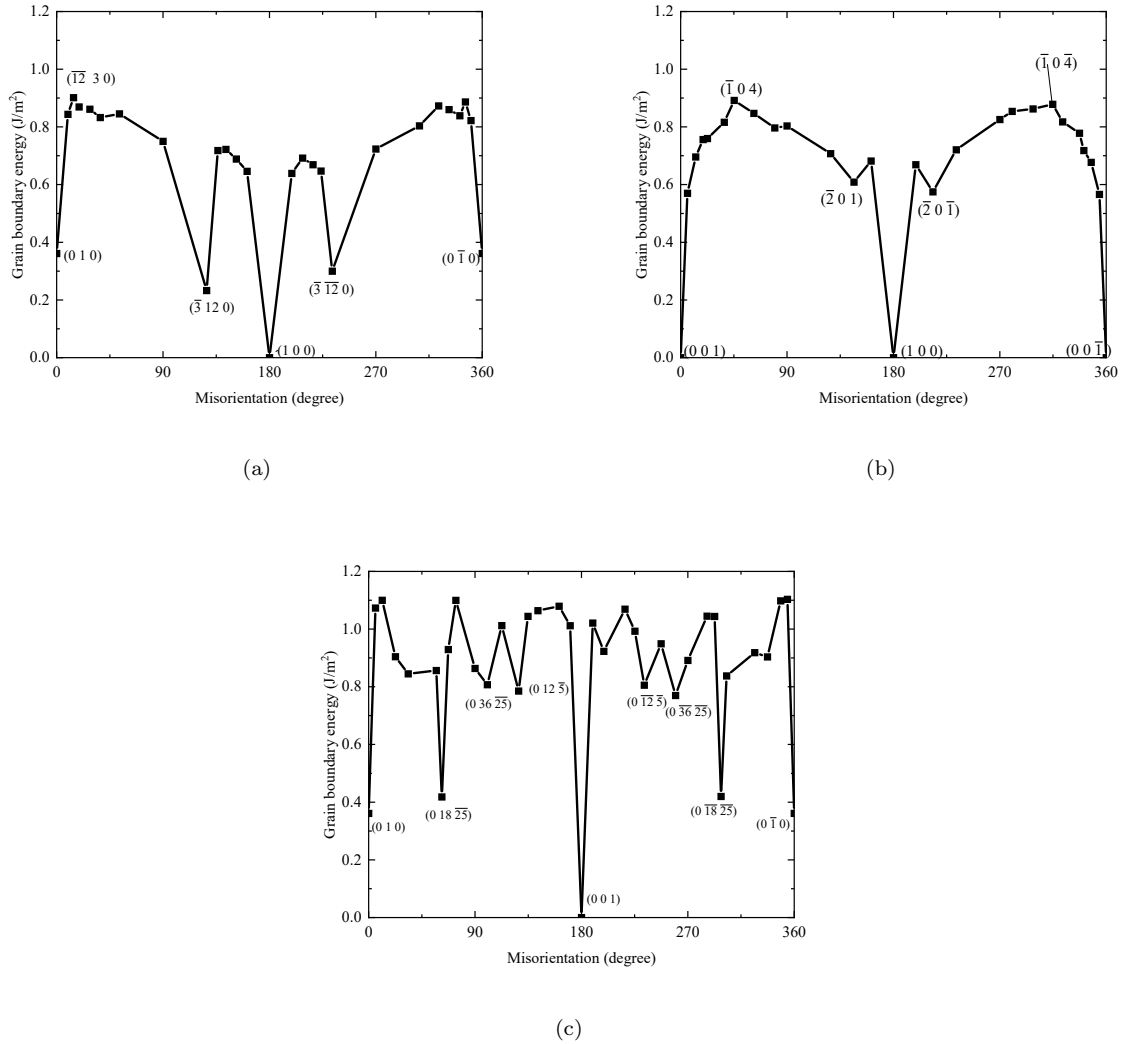


Figure 3: Grain boundary energy of STGB (symmetric tilt grain boundary) of (a) type A, (b) type B, and (c) type C as a function of misorientation angles at 500 K. Key features are labeled with their STGB plane orientation.

to the symmetry of the $(1\ 0\ 0)$ and $(0\ 0\ 1)$ planes of α -U, hence the major cusps with a value of zero located at these orientations. Type B STGBs have a simple arithmetic average GB energy of $0.75\ \text{J/m}^2$. This type
 175 has a mirror symmetry of STGB energy profile with respect to the $(1\ 0\ 0)$ plane similar to type A STGB, see Figure 3(b) and (a), which complies with crystallographic theory.

Type C STGBs ($\langle 0\ 0\ 1 \rangle$ tilt axis) have the highest number of cusps (eight), which are oriented at a mirror
 180 symmetry orientation with respect to the $\langle 0\ 0\ 1 \rangle$ tilt axis (see Figure 3(c)) over the 0° to 360° misorientation angle domain. Apart from the mirror symmetry, there is no discernible trend for GB energy of type C STGB as a function of misorientation angle. In the 0° to 180° misorientation angle domain, the major cusp is at the $(0\ 1\ 0)$ and $(0\ 18\ \bar{2}5)$ planes, and minor cusps exist at the $(0\ 36\ \bar{2}5)$ and $(0\ 12\ \bar{5})$ planes. The corresponding GB plane energies are $0.36\ \text{J/m}^2$, $0.40\ \text{J/m}^2$, $0.79\ \text{J/m}^2$, and $0.8\ \text{J/m}^2$, respectively. The $(0\ 1$

0) and $(0 \bar{1} 0)$ orientations have misorientation angles of 0° and 360° , respectively, and because of α -U having no mirror symmetry with respect to the $(0 1 0)$ plane, these planes contain GBs with a very small atomic misfit. Because of the low GB energy, $(0 18 \bar{2}\bar{5})\langle 0 0 1 \rangle$ STGB could be a probable twinning orientation of α -U. No statistically significant highest GB energy among type C STGBs is found. Like type A, at the 180° misorientation angle there is no grain boundary and zero GB energy because of the symmetry of the $(0 0 1)$ plane of α -U. Type C STGBs have an average GB energy of 0.89 J/m^2 considering all the cusps. Excluding the major cusps (probable twinning orientations), the average GB energy of the general type C STGBs is 0.96 J/m^2 .

This study indicates that general type C STGBs have the highest average GB energy, followed by general type A STGBs, with type B STGBs exhibiting the lowest grain boundary energies. Among the entire dataset of eighty STGBs, the lowest GB energy is observed for the type A STGB at the $(\bar{3} 12 0)\langle 1 0 0 \rangle$ STGB plane, where $(0 1 0)$ is the tilt plane, $(0 0 1)$ is the shear plane, and the GB energy is 0.27 J/m^2 , followed by a type C STGB at the $(0 18 \bar{2}\bar{5})\langle 0 0 1 \rangle$ STGB plane, where $(0 1 0)$ is the tilt plane, $(1 0 0)$ is the shear plane, and the GB energy is 0.42 J/m^2 . These two could be a probable twin orientation for α -U, though neither has been observed experimentally yet. To date, the two most prominent twinning modes have been observed to be the $\{1 3 0\}\langle 3 \bar{1} 0 \rangle$ and the $\{1 7 2\}\langle 3 \bar{1} 2 \rangle$ [18, 20, 39, 40]. Though $\{1 1 2\}\langle 3 \bar{7} 2 \rangle$ twins have the same shear factor as $\{1 7 2\}\langle 3 \bar{1} 2 \rangle$, they exhibit a low prevalence in experimental investigations of polycrystalline α -U [18, 20, 40, 41]. Additional twin modes with orientations of $\{2 1 0\}$ and $\{1 7 6\}$ have been discovered with electron microscopy techniques [42, 43]. Though the $\{1 1 0\}$ twin has a low shear factor, it typically does not appear experimentally because this shear plane also acts as one of the dominant slip systems [20].

As no data on GB energies in α -U are available for comparison, the current computational work is compared with previous computational studies of γ -U, U_3Si_2 , and UO_2 . γ -U has a BCC crystal structure, while U_3Si_2 has a somewhat complex two sublattice tetragonal structure, and UO_2 has a fluorite structure. γ -U [44] was found to have a lower grain boundary energy than U_3Si_2 [36] at 600 K for the misorientation domain 0° to 90° . For this orientation region and temperature (analogous to the type A STGB in this work), γ -U has a GB energy from 0.3 J/m^2 - 0.45 J/m^2 , whereas U_3Si_2 has a GB energy in the range of 0.7 J/m^2 - 1.2 J/m^2 . Under the same conditions, α -U STGBs possess a GB energy from 0.27 J/m^2 - 0.87 J/m^2 . Thus, there are good quantitative comparisons for GB energies amount these three U-based systems. At 300 K, ceramic UO_2 has a GB energy between 1.0 and 3.0 J/m^2 , for a range of misorientation angles of 10° to 62° [25]. From the present work at 300 K (shown in the subsequent section), α -U shows an average GB energy of approximately 0.79 J/m^2 . Hence, compared to UO_2 , α -U STGBs exhibit significantly lower GB energies at 300 K.

From Fig. 3, it is observed that the GB energy of α -U not only depends on the misorientation angle but also on the tilt plane and shear plane. This variation in GB energy is quantified here as the grain boundary anisotropy. Equation 3 refers to GB energy anisotropy ($GBAniso_{\text{TYPE}}$) for a fixed misorientation angle (θ), comparing the three types of GBs, and Equation 4 compares all misorientation angles (θ) for a given type

of GB to evaluate GB anisotropy ($GBAniso_{\theta}$) due to variation of misorientation angles.

$$GBAniso_{TYPE} = \left(\frac{\max(GB_E) - \min(GB_E)}{\max(GB_E)} \right)_{\theta} \quad (3)$$

$$GBAniso_{\theta} = \left(\frac{\max(GB_E) - \min(GB_E)}{\max(GB_E)} \right)_{TYPE} \quad (4)$$

To compare the dependency of the GB anisotropy on GB types ($GBAniso_{TYPE}$), seven misorientation angles (12.8°, 35.7°, 60°, 90°, 126.9°, 144.3° and 161.08°) are considered for each of the three types of STGBs (Figure 4). For instance, STGB $(\bar{3} 6 0)(1 0 0)$ from type A, STGB $(\bar{3} 0 5)(0 0 1)$ from type B, and STGB $(0 6 \bar{5})(0 0 1)$ from type C, all have the same misorientation angle of 90°. The maximum and minimum GB energy of these three planes are considered in order to evaluate the anisotropy in GB energy for the 90° misorientation due to the change in the tilt plane and shear plane (STGB type). It can be seen that as the misorientation angle increases, the anisotropy across grain boundary types qualitatively increases (Figure 4). Thus, at a high misorientation angle, the type of tilt and shear axes are more critical in determining the grain boundary energy. This is a general relationship, and likely does not hold for special cusps in the grain boundary landscape. At the cusp orientations (60° and 126.9°) $GBAniso_{TYPE}$ becomes very large, as cusps (or preferred twinning orientations) for all types of STGBs are not formed at the same misorientation angle due to anisotropic structure of α -U.

To determine the GB energy anisotropy for a fixed STGB type (for instance, type A STGBs) due to change in misorientation angle ($GBAniso_{\theta}$), all twenty-six type A STGBs considered. The maximum and minimum GB energy are input into Equation 4, yielding three data points which are not shown in Figure 4 (one for each type STGB). The lowest anisotropy among the STGB types due to variation has been found in type B STGBs, with a value of 0.4, while type A and type C display a comparable amount of anisotropy (approximately 0.7). This qualitatively corresponds to the number of cusps and their magnitude, as observed in Figure 3. Typically, there exists a greater degree of GB energy anisotropy due to misorientation angle, rather than the underlying tilt and shear axes.

To grasp the mechanisms governing the anisotropic grain boundary properties, we must approach the problem from the perspective of the unique crystal structure of α -U. From a crystallographic point of view, α -U consists of corrugated planes parallel to the $(0 1 0)$ plane. These corrugated planes are compressed with respect to the $\langle 0 0 1 \rangle$ direction, meaning that the corrugation direction is $\langle 0 0 1 \rangle$ and $\langle 1 0 0 \rangle$ is the transverse direction of corrugation. When $(1 0 0)$ is designated as the shear plane (type C) to generate an STGB, continuity of the corrugated planes at the interface (or tilt plane $(0 1 0)$) is interrupted. As a result, at the interface, all bonds in the corrugated direction are broken and need to be reconstructed. For type B STGBs, corrugated planes of α -U are parallel to the shear plane $(0 1 0)$. Therefore, the bonds that need to be reconstructed are located in the same corrugated planes. Finally, for type A STGBs, the shear plane is $(0 0 1)$ while $(0 1 0)$ is the tilt plane (or cut plane), and corrugated planes are perpendicular to the shear plane. In order to generate a type A STGB, bonds oriented in the transverse direction of the corrugation have to be reconstructed. It should be reiterated that type C STGBs have the highest average GB energy, followed

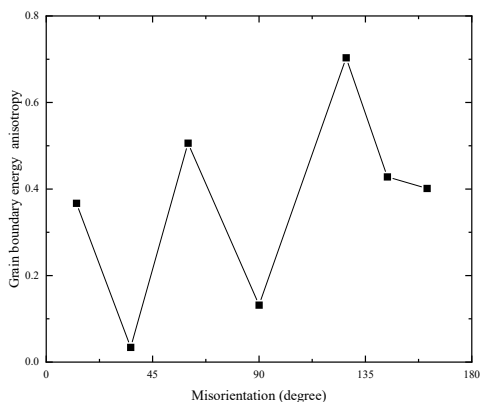


Figure 4: Grain boundary energy anisotropy ($GBAniso_{TYPE}$) in selected STGBs of α -U at 500 K. Anisotropy here is considered as a function of GB type (type A STGB, type B STGB and type C STGB).

by type A STGBs, with type B STGBs exhibiting the lowest grain boundary energies, which corresponds to a corrugated plane bonding conceptual framework. From this computational work, it is observed that both the degree and type of bond reconstruction along corrugated planes, in addition to the atomic misfit within the interface, are important to determine the GB energy of an STGB. Further analysis of GB structure using different methodologies can confirm the change of GB energy with misorientation angle, shear plane, and temperature [45, 46].

3.1.2. Effect of temperature

To study the effect of temperature on GB energy of α -U STGBs, twenty-two STGBs (eight from type A, seven from type B, and seven from type C) are selected for further analysis. The studied temperatures are 300 K, 400 K, 500 K, and 600 K. The GB energy as a function of temperature for different orientations is presented in Figure 5. To evaluate the temperature sensitivity, the lowest studied temperature, 300 K, is considered as the reference point.

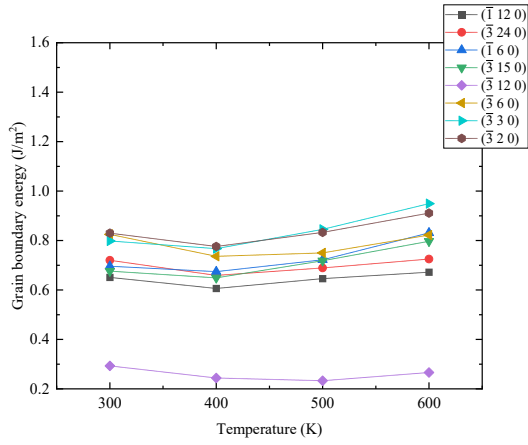
From Figure 5(a), in general, there is a decreasing trend of the GB energy of type A STGBs up to 400 K, followed by an increasing trend up to 600 K. The minimum grain boundary energy occurs for the $(\bar{3} 12 0)$ plane at all temperatures (the arithmetic average of GB energy of this plane is 0.25 J/m^2 over the temperature range). However, the maximum energy STGB is not the same for all temperatures studied. The maximum grain boundary energy occurs at the $(\bar{3} 2 0)\langle 1 0 0 \rangle$ at 300 K and 400 K, but occurs at the $(\bar{3} 3 0)\langle 1 0 0 \rangle$ at 500 K and 600 K. The $(\bar{3} 12 0)\langle 1 0 0 \rangle$ orientation is also the lowest energy type A STGBs in Figure 3(a). The $(\bar{3} 3 0)\langle 1 0 0 \rangle$ STGB shows the largest dependency on temperature, as its value varies by 0.18 J/m^2 over the temperature range. The lowest temperature sensitivity is observed at the $(\bar{1} 12 0)\langle 1 0 0 \rangle$, $(\bar{3} 1 12 0)\langle 1 0 0 \rangle$, and $(\bar{3} 24 0)\langle 1 0 0 \rangle$ STGB, where the GB energy varies by 0.07 J/m^2 over the studied temperature range. The average change in GB energy over the studied temperature range is observed to be

275 0.11 J/m² (14.5%) with respect to GB energy at room temperature.

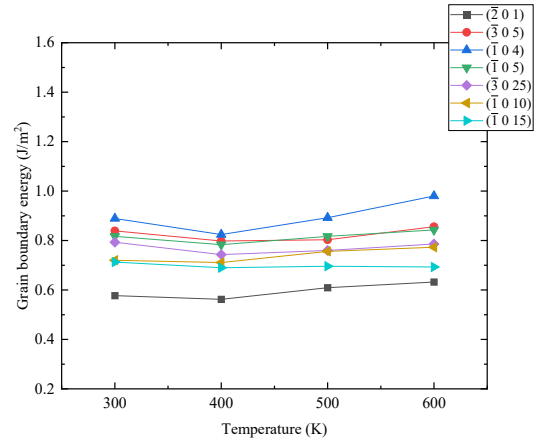
Type B grain boundaries (Figure 5(b)) show a behavior similar to that of the type A grain boundaries. For nearly all of the studied planes the lowest energy is attained at 400 K, while the highest energy is observed at 600 K. The $(\bar{2} 0 1)$ plane has the lowest energy at every temperature (average over temperature range 0.59 J/m²). The $(\bar{1} 0 15)$ plane displays the least variation with temperature among those studied
280 (0.02 J/m²). The $(\bar{1} 0 4)\langle 0 0 1 \rangle$ STGB exhibits the highest GB energy at all studied temperatures, and the largest dependency on temperature as its value varies by 0.16 J/m². The average change in GB energy over the studied temperature range with respect to GB energy at 300 K is observed to be 0.07 J/m², or 6%.

For type C STGBs, the grain boundary energy shows an increasing trend with temperature, which accelerates with increasing temperature, see Figure 5(c). For example, the $(0 72 \bar{25})\langle 0 0 1 \rangle$ STGB shows an
285 increase of grain boundary energy from 300 K to 400 K of 4%, from 400 K to 500 K of 24.3%, and from 500 K to 600 K of 39.4%. Among the grain boundary planes, the $(0 18 \bar{25})$ plane exhibits the lowest GB energy at each temperature studied (the average GB energy over the temperature range studied for this plane is 0.42 J/m²). At both 300 K and 400 K, the maximum grain boundary energy is observed for the $(0 36 \bar{5})$ plane, while, at both 500 K and 600 K, the maximum grain boundary energy is observed for the $(0 9$
290 $\bar{10})$ plane. The $(0 6 \bar{5})$ plane has the least dependency on temperature as it varies by 0.44 J/m², or 45.9% from the GB energy at 300 K, followed by the lowest energy STGB $(0 18 \bar{25})\langle 0 0 1 \rangle$ which increases by 0.48 J/m², but this increase equates to a 175% increase from the GB energy at 300 K. The $(0 9 \bar{10})\langle 0 0 1 \rangle$ STGB experiences the highest change with temperature, of 0.66 J/m². The average change in GB energy over the studied temperature range is observed to be 82% (0.56 J/m²) from the reference energy at 300 K. Compared
295 to type A and B grain boundaries, type C is significantly more temperature-sensitive.

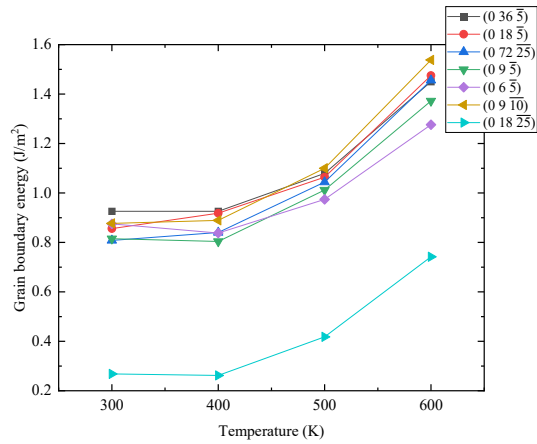
The current work generally finds that for α -U STGBs, the GB energy is positively correlated with temperature (specifically from 400 K to 600 K). The temperature dependence of type C STGBs is similar to results for type A STGB of U₃Si₂ [36], and this trend is also observed in γ -U type A STGBs [36]. However, the GB energy of α -U STGBs is more temperature-sensitive than UO₂, as the GB energy of UO₂ changes
300 by only about 7% from 300 K to 600 K [47]. The current work indicates that at lower temperatures, there is less driving force for grain growth due to the lower grain boundary energy, as GB velocity is proportional to driving force (which is dependent upon the GB energy [13]). This can lead to a relatively stable fine-grained microstructure, which can hinder dislocation movement and can lead to lower ductility within the material. Combined with a fine-grained microstructure, high stresses associated with twinning may not be relieved by
305 slip, possibly reducing α -U ductility. Experimental evidence indicates that below 573 K, twinning activities of α -U increase with decreasing temperature, down to 198 K [17, 48, 49]. From the current work, the GB energy of two probable twinning orientations, $(\bar{3} 12 0)\langle 1 0 0 \rangle$ and $(0 18 \bar{25})\langle 0 0 1 \rangle$ has a positive relation with temperature from 400 K to 600 K and from 300 K to 600 K, respectively, and both exhibit less temperature sensitivity with respect to room temperature than other general STGBs of their respective type (type A and
310 C).



(a)



(b)



(c)

Figure 5: Grain boundary energy of selected STGBs of (a) type A, (b) type B, and (c) type C as a function of temperature

3.2. Surface Energies

3.2.1. Effect of tilt angle

In this section, the dependence of surface energy on tilt angle is discussed. The surfaces considered in this work are only those which are related to the STGBs. For instance, a STGB characterized by $(\bar{3} 6 0)\langle 1 0 0 \rangle$ will be analyzed as a surface characterized by $(\bar{3} 6 0)$. The effect of tilt angle (surface orientation) on the surface energy of type A, type B, and type C surfaces is plotted in Figure 6. The surface energies of the $(1 0 0)$, $(0 1 0)$, and $(0 0 1)$ planes have also been evaluated. The tilt angle of the studied surfaces ranges from 0° to 180° and the energies are characterized at 500 K. Data points are connected by straight lines to guide the eye.

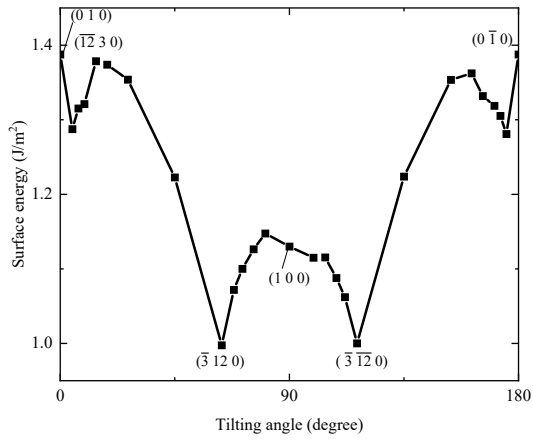
Type A surfaces have an average surface energy of 1.25 J/m^2 , with the minimum energy surface observed for the $(\bar{3} 12 0)$ (symmetric $\bar{3} \bar{12} 0$) plane, at 1.0 J/m^2 . Interestingly, the $(\bar{3} 12 0)\langle 1 0 0 \rangle$ STGB also has the lowest GB energy of type A. The maximum type A surface energy is observed within a range of 1.35 J/m^2 to 1.38 J/m^2 , whereas the surface energy of the $(0 1 0)$ surface is slightly higher (1.39 J/m^2). The shear plane for a type A STGB is $(0 0 1)$ and this plane has 1-fold symmetry. Because of this, there is mirror symmetry in the surface energy plot as a function of tilt angle (Figure 6(a)) and the GB energy as a function of misorientation angle (Figure 3(a)) along the $\langle 1 0 0 \rangle$ tilt axis. The general trend of surface energy (from 0° to 90°) is to increase from a small tilt angle 5° up to 15° , then decrease until 65° , followed by an increase up to 90° .

Like type A surfaces, a mirror symmetry with respect to tilt angle 90° is apparent in Figure 6(b) for type B surfaces, though a more simplified general trend is found. The surface energy increases up to 30° , followed by a decrease up to 90° . This occurs because of the 180° rotational symmetry with respect to the diagonal direction of the $(0 1 0)$ plane, and the $(0 1 0)$ is the shear plane of type B STGBs of the α -U unit cell. The highest energy surface is the $(\bar{9} 0 25)$ plane (identical to the $(\bar{9} 0 \bar{25})$ plane), having a surface energy of 1.30 J/m^2 . The lowest energy has been observed for the $(0 0 1)$ plane with a surface energy of 1.11 J/m^2 , and the second-lowest energy surface is $(1 0 0)$ with a value of 1.13 J/m^2 . The average surface energy of type B was found to be 1.21 J/m^2 . Among the three types of studied surfaces, type B has the least sensitivity to surface tilt angle and the lowest average surface energy.

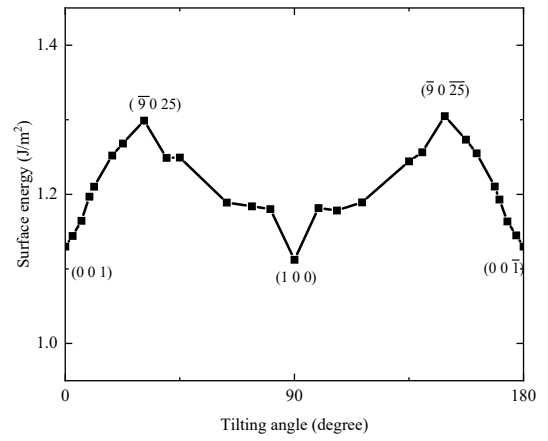
Type C surface energies as a function of tilt angle at 500 K are shown in Figure 6(c). Due to the 1-fold symmetry along of the $(1 0 0)$ shear plane of the α -U unit cell, there is mirror symmetry in the surface energy plot. The general trend of type C surfaces is somewhat similar to that observed for type A surfaces, in that there is a decrease up to 35° , then an increase until 65° , but then followed by a decrease up to 90° . However, there is neither any statistically significant low energy nor any high energy surface that can be observed for type C surfaces. The lowest surface energy ranges between 1.10 J/m^2 and 1.11 J/m^2 for three surfaces, including the $(0 \bar{9} \bar{10})$, $(0 9 \bar{10})$, and $(0 0 1)$ planes. The highest surface energies exist among the $(0 \bar{72} \bar{25})$ (or symmetric $(0 \bar{72} \bar{25})$), and $(0 1 0)$ planes, ranging between 1.36 J/m^2 and 1.39 J/m^2 . Similar to type C STGBs (Figure 3(c)), type C surfaces exhibit the highest average surface energy at 1.26 J/m^2 with

respect to the other two types.

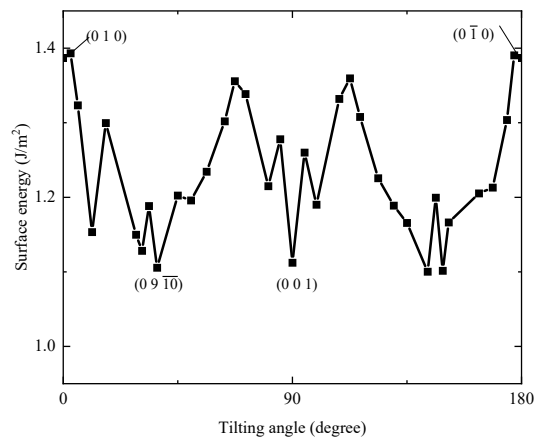
Mirror symmetries that have been observed in all three types of surfaces match with the crystallography of the corresponding shear planes. Type A, B, and C surfaces have an average surface energy larger than their corresponding GB energy by 39.3%, 38%, and 22.7%, respectively. In a recent study, the surface energy of seven basic surfaces in α -U was calculated using density functional theory [29]. Among these surfaces, the (0 0 1) surface possesses the lowest energy, which agrees with the findings from the current work. However, the magnitude of the surface energy in this work does not directly correspond to the work in [29], where the (0 0 1) surface energy was characterized as 1.76 J/m², while our results indicate a surface energy of 1.11 J/m². However, the global arithmetic average of all surface energies calculated for the STGBs in this work is 1.23 J/m², which falls within the range of available computational data on the surface energy of α -U [26, 28, 29, 50]. Comparing to other fuel systems, the magnitude of the average surface energy of α -U (approximately 1.23 J/m²) is higher than the γ -U [44] surface energy (1.15 J/m²) at 600 K, while it is lower than the surface energy of U₃Si₂ [36] (approximately 1.78 J/m²) at the same temperature. The surface energy of {1 0 0} planes in UO₂ have been observed to be between 1.69 J/m² and 1.92 J/m² (calculated utilizing MD [25]) at 300 K. This is higher than the (1 0 0), (0 1 0) and (0 0 1) surfaces of α -U at 500 K from this work, which is similar to the comparisons between the GB energies between the two materials.



(a)



(b)



(c)

Figure 6: Surface energy of surfaces of (a) type A, (b) type B, and (c) type C as a function of tilt angle at 500 K.

3.2.2. Effect of temperature

An investigation of surface energy variation with temperature is performed, similar to the investigation
365 of GB energy with temperature. In Figure 7, surface energies of type A, B, and C surfaces are displayed as a
function of temperature. To study the effect of temperature on surface energy, a subset of eight planes have
been chosen from type A, seven from type B, and seven from type C. All of these planes range between 0°
and 90° misorientation angle.

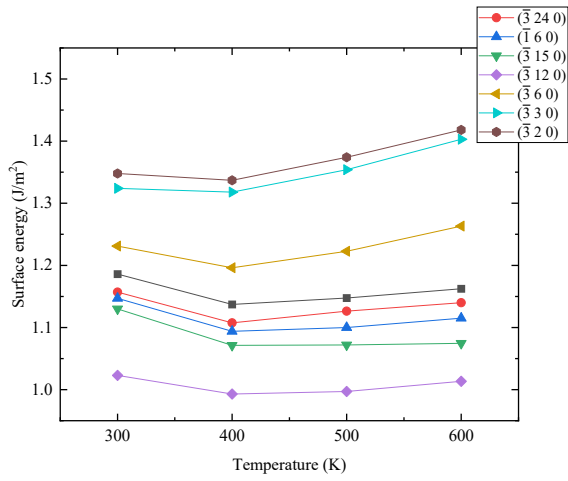
From Figure 7(a), the common trend of temperature dependency of type A STGB surfaces is a decrease
370 from 300 K to 400 K, followed by a linear increase up to 600 K. The rate of increase depends upon the surface
orientation. The $(\bar{3} 12 0)$ plane exhibits the lowest surface energy over the entire temperature range, and
the $(\bar{3} 2 0)$ plane exhibits the highest surface energy over nearly the entire temperature range. The surface
planes $(\bar{3} 12 0)$ and $(\bar{3} 2 0)$ have an average surface energy over the temperature range of 1.01 J/m^2 and
 1.37 J/m^2 , respectively. The smallest dependency on temperature has been observed at the $(\bar{3} 12 0)$ surface
375 plane (varying by a maximum of 0.03 J/m^2) and the greatest dependency at the $(\bar{3} 3 0)$ plane (varying by
a maximum of 0.09 J/m^2).

Type B surfaces in Figure 7(b) typically display a slight decrease in the surface energy from 300 K to
400 K, followed by an increase in surface energy up to 600 K, though the variation with temperature is
noticeably less than either type A or type C surfaces. The $(\bar{1} 0 15)$ plane consistently exhibits the lowest
380 surface energy with an average value of 1.17 J/m^2 , and the $(\bar{1} 0 4)$ plane has the highest surface energy with
an average value of 1.27 J/m^2 over the temperature range. The average change in surface energy from 300
K to 600 K is observed to be 2.5% for this subset of surfaces. The most temperature-sensitive surface is the
 $(\bar{1} 0 5)$ plane, showing an increase of 0.07 J/m^2 , while the least temperature-sensitive surface is the $(\bar{1} 0 10)$
plane, which varies by 0.04 J/m^2 over the studied temperature range.

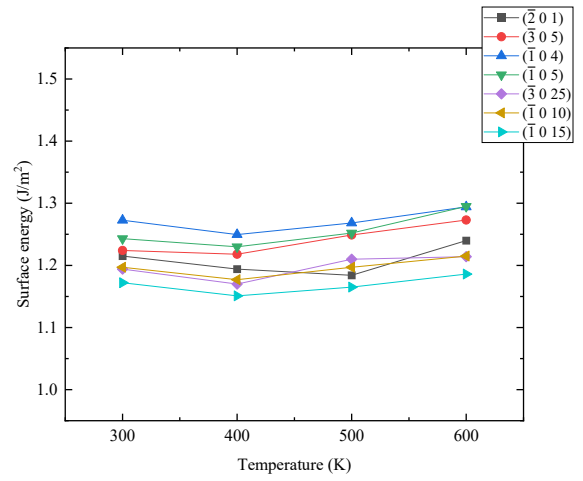
All the studied surfaces of type C exhibit the highest surface energy at 600 K. The $(0 9 \bar{5})$, $(0 6 \bar{5})$, and
385 $(0 9 \bar{10})$ planes have their lowest surface energy at 400 K, though, their energy is lower by only 0.01 J/m^2
from the respective value at 300 K. The rest of the surface planes studied attain a minimum energy at 300
K. Therefore, it can be said that type C surfaces have a trend of increasing surface energy with increasing
temperature 7(c). This trend is similar to that observed in the type C STGBs, but the rate of increase is
390 slower than that of the corresponding type C STGBs. For example, the $(0 72 \bar{25})$ plane shows an increase
of surface energy from 300 K to 400 K of 1.1%, from 400 K to 500 K of 7.2%, and from 500 K to 600 K
of 12.8%, see Figure 7(c). The corresponding percentage increases of the $(0 72 \bar{25})(0 0 1)$ STGB energy are
4%, 24.3%, and 39.4%, see Figure 5(c). The $(0 18 \bar{25})$ surface displays the lowest surface energy over the
entire temperature range with an average value of 1.13 J/m^2 , and the $(0 72 \bar{25})$ plane displays the highest
395 surface energy among all the studied seven planes with an average value of 1.35 J/m^2 . The $(0 9 \bar{10})$ plane
has the least sensitivity to temperature, as it varies by only 0.03 J/m^2 over the temperature range. The $(0$
 $72 \bar{25})$ plane varies by 0.28 J/m^2 over the temperature range, which is maximum among the studied type C
surfaces. Comparing with the other two types of surfaces, type C surfaces are significantly more sensitive to

temperature.

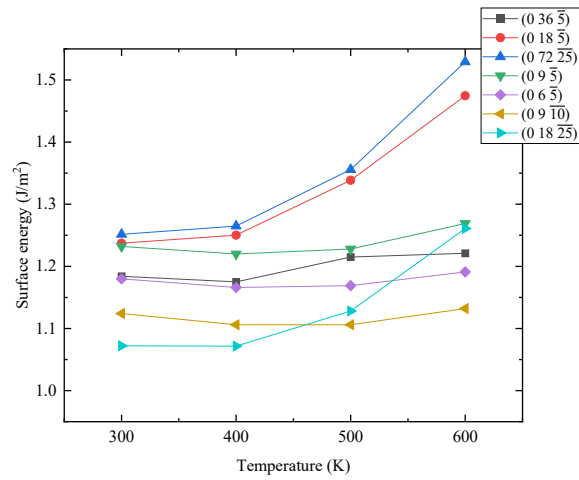
400 When considering the average variation in surface energy with temperature, type C STGBs in α -U have a similar trend to γ -U surfaces [44]. However, the trend of surface energy for type A and B surfaces in α -U is more similar to U_3Si_2 surface energies [36]. The surface energy change from 300 K to 600 K for type A and B STGBs shows that they possess a smaller temperature dependency than UO_2 , which was observed to be 7.4% [47], whereas type C shows a stronger dependency on temperature.



(a)



(b)



(c)

Figure 7: Surface energy of selected surfaces of (a) type A, (b) type B, and (c) type C as a function of temperature.

405 3.3. Work of adhesion for α -U

3.3.1. Effect of misorientation angle

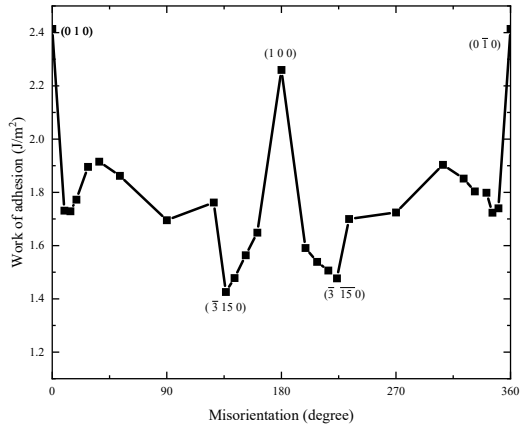
The work of adhesion (WAd) of different STGBs at 500 K is calculated via Equation 2 and plotted as a function of the corresponding misorientation angle in Figure 8. The WAd is defined here as the energy required to form two surfaces from a given STGB. A lower value for the work of adhesion represents less
410 total energy required to break apart a GB into two separate free surfaces. Thus, orientations with low WAd are potential sites for cleavage or fracture, or the nucleation of the α tearing phenomenon [21].

Before explaining Figure 8, it should be emphasized that in all types of STGBs, the (1 0 0) and the (0 0 1) planes represent the pure crystalline system, with no true GB present. Thus, the WAd values for the (1 0 0) and (0 0 1) planes (2.26 J/m² and 2.22 J/m², respectively) are the WAd values of the perfect crystal
415 system, which is simply two times the surface energy of the (1 0 0) or (0 0 1) plane. Conversely, grain boundaries are observed at the (0 1 0) misorientation plane because of the absence of mirror symmetry with respect to this plane. This is why, for misorientation angles of 0° or 360° in type A and C STGBs, GBs are formed. Like the GB energy analysis, here STGBs having misorientation angles between 0° to 180° are discussed.

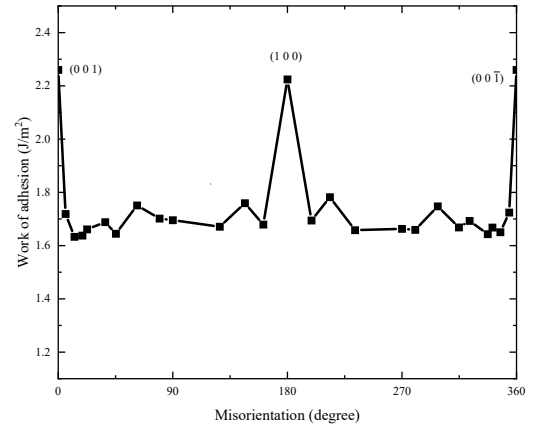
The maximum WAd of type A STGBs has been found for the (0 1 0) STGB and the minimum for the ($\bar{3}$ 15 0) STGB, with magnitudes of 2.4 J/m² and 1.43 J/m², respectively, as seen in Figure 8(a). In order to split an STGB of type A into two type A surfaces, an average of 1.78 J/m² of energy is required. For type B orientations, no statistically significant minimum or maximum is observed, as all the WAd values reside from 1.6- 1.8 J/m² (see Figure 8(b)). Type C STGBs exhibit the lowest average WAd from the three plane
425 types, whereas type C STGBs and surfaces exhibit the highest GB and surface energies. The highest WAd is found for the (0 1 0) plane (2.41 J/m²), while the lowest WAd is observed for the (0 9 $\bar{10}$) plane (mirror of the (0 $\bar{9}$ $\bar{10}$) plane), at 1.11 J/m² (Figure 8(c)).

The WAd for type B STGBs is less sensitive to misorientation angle, as WAd values fluctuate within a very small range (1.6-1.8 J/m²) compared to type A and C STGBs. Type B STGBs have an average WAd of
430 1.75 J/m², while type A STGBs have an average WAd of 1.78 J/m², and type C STGBs an average of 1.61 J/m². Aside from the mirror symmetry with respect to the tilt plane, there are no distinguishable patterns observed in the WAd profile of the studied STGBs of α -U.

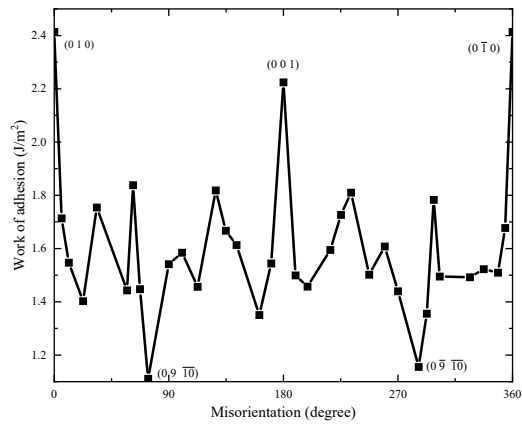
Two possible twins in α -U found from the current study are the ($\bar{3}$ 12 0)(1 0 0) STGB and the (0 18 $\bar{25}$)(0 0 1) STGB. Although these STGBs are found to have very low energies, their WAd values are not
435 significantly higher or lower than the average WAd of the respective type of STGB. The WAd of these STGBs are 1.76 J/m² and 1.83 J/m², respectively. Among all the studied STGBs, ($\bar{3}$ 2 0)(1 0 0) has the maximum resistance to failure (except the (1 0 0), (0 0 1), and (0 1 0) misorientation planes) with a WAd of 1.92 J/m², whereas the most susceptible orientation for failure is the (0 9 $\bar{10}$)(0 0 1) STGB, with a WAd of 1.11 J/m². The GB energy of this orientation is also 1.11 J/m². The difference in misorientation angle
440 between a probable twinning orientation of type A STGB, ($\bar{3}$ 12 0)(1 0 0), and a probable failure site, ($\bar{3}$ 15



(a)



(b)



(c)

Figure 8: Work of Adhesion of STGBs of (a) type A, (b) type B, and (c) type C as a function of misorientation angle at 500 K.

0) \langle 1 0 0 \rangle , is approximately 10°. Like type A STGBs, a probable twinning site of type C STGBs ($(0\ 18\ \bar{2}5)\langle$ 0 0 1 \rangle) resides within 10° misorientation angle of a probable failure site ($(0\ 9\ \bar{1}0)\langle$ 0 0 1 \rangle).

The α -U WAd values can be compared with the available literature on the WAd of other fuel systems. At 300 K, the cleavage energy of UO₂ [25] GBs has a wide range, from 0.3 J/m² to 2.5 J/m² (maximum of 4.5 J/m² in Reference [51]). The work presented here demonstrates an approximate average WAd of 1.91 J/m² at 300 K, suggesting that the WAd of α -U STGBs is likely to be within the upper range of UO₂. α -U has a lower average WAd at 600 K (approximately 1.68 J/m²) than γ -U (approximately 1.9 J/m²) and U₃Si₂ (approximately 2.6 J/m²) [44, 36]. Hence, α -U is more prone to failure along GBs compared to other uranium-based nuclear fuels.

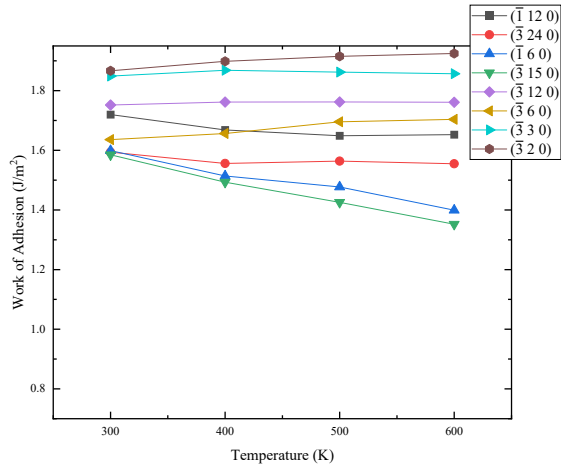
3.3.2. Effect of temperature

Similar to GB energy and surface energy, the effect of temperature on WAd of α -U is investigated. For this analysis, twenty-two STGBs (eight from type A, seven from type B, and seven from type C) are selected for further analysis. The studied temperatures are 300 K, 400 K, 500 K, and 600 K; among them, 300 K is considered as the reference point to evaluate the temperature sensitivity. The WAd as a function of temperature for different STGBs is presented in Figure 9.

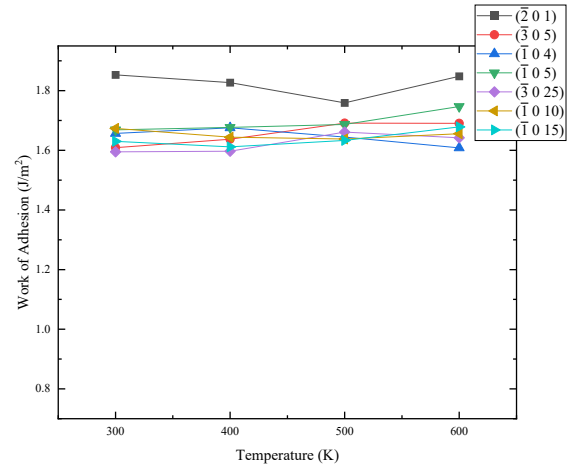
From Figure 9(a), it is observed that unlike GB energy and surface energy of type A STGBs, WAd has an inverse relationship with temperature when the misorientation angle is greater than 130° (see Appendix Table 1 for associated misorientation angles). The least temperature-sensitive (only 0.01 J/m²) STGB of type A is the $(\bar{3}\ 12\ 0)\langle$ 1 0 0 \rangle . However, the WAd changes by a maximum of 0.23 J/m² for the $(\bar{3}\ 15\ 0)\langle$ 1 0 0 \rangle STGB, which has the lowest WAd among all studied type A STGBs, with an average WAd of 1.46 J/m² over the temperature range. The highest WAd among the studied subset of type A STGBs is observed at the $(\bar{3}\ 2\ 0)$ plane, with an average WAd of 1.9 J/m² across all temperatures. Moreover, this plane also exhibits the highest surface energy at all temperatures. For a misorientation angle less than or equal to 130°, the increase in the WAd with temperature is not significant (maximum by 0.07 J/m² for STGB $(\bar{3}\ 6\ 0)\langle$ 1 0 0 \rangle).

Similar to both type B STGB and surface energies (see Figure 7(b)), type B WAd shows only minimal variance (maximum of 5.3%) with temperature, see Figure 9(b). The maximum variation is observed for the $(\bar{2}\ 0\ 1)\langle$ 0 0 1 \rangle STGB, which shows an increase of 0.09 J/m² with temperature. However, this increasing trend is not consistent for other planes, where some planes instead show a decrease in WAd with increasing temperature. The least sensitivity is found for the $(\bar{1}\ 0\ 10)$ plane, which varies by 0.04 J/m². Among the seven type B STGBs studied, the range of WAd values decreases with temperature. For instance, at 300 K the WAd has a range (maximum minus minimum) of 0.21 J/m², which is reduced with increasing temperature until it becomes 0.14 J/m² at 600 K. From this evidence, we can say that the dependence of WAd on misorientation angle is stronger at lower temperatures for type B STGBs.

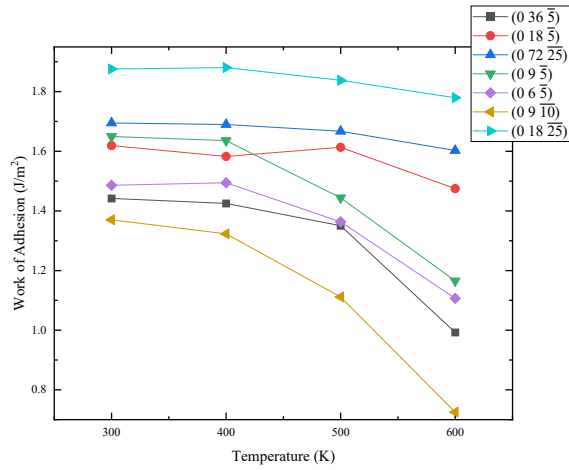
The general trend of the WAd of type C STGBs is to decrease with temperature, as seen in Figure 9(c). The $(0\ 9\ \bar{1}0)\langle$ 0 0 1 \rangle STGB shows the highest percentage (47%) decrease (0.65 J/m²) of WAd with respect to the corresponding WAd at 300 K and also has the lowest WAd among the type C STGBs, see Figure



(a)



(b)



(c)

Figure 9: Work of Adhesion of selected STGBs of (a) type A, (b) type B, and (c) type C as a function of temperature.

8(c), with an average WAd over the temperature range of 1.13 J/m². The least temperature sensitivity (0.1 J/m²) is observed for the (0 18 $\bar{2}5$) \langle 0 0 1 \rangle STGB, which is one of the preferred twinning orientations. At all the studied temperatures, the (0 18 $\bar{2}5$) plane shows the highest WAd value (average WAd is 1.84 J/m²) while the GB energy for this orientation is the lowest for all temperatures, see Figure 5(c).

Similar to GB energy, the WAd of two preferable twinning sites ($\bar{3}$ 12 0) \langle 1 0 0 \rangle and (0 18 $\bar{2}5$) \langle 0 0 1 \rangle shows less dependency on temperature than general STGBs of type A and C, respectively. We recall from Fig. 5 and 7 that the grain boundary energy increases with temperature (type A 14.5%, type B 6.6% and type C 82.2%) at a higher rate than the surface energy (type A 4.4%, type B 2.6% and type C 10.2%). Given this relationship and equation 2, the general trend of WAd is to decrease with temperature. This indicates that in general it is expected to require slightly less work to create two surfaces from an STGB as the temperature increases, which means α tearing is more favorable at higher temperatures. This finding is also consistent with the literature [22, 52]. During irradiation, the anisotropic irradiation growth of individual grains in polycrystalline α -U generates stress concentrations at grain boundaries [53]. Additionally, anisotropic thermal expansion can generate additional internal stresses [34]. Due to these stress concentrations, micro-tearing may take place at the grain boundaries, generating void space and swelling [52]. At temperatures below about 623 K, polycrystalline α -U deforms plastically without the loss of density, but at temperatures of approximately 623 K to 723 K, a deformed microstructure with ragged cavities (indicative of grain boundary failure) occurs. This behavior is specific to irradiated α -U, though similar behavior is evident during thermal cycling [22].

4. Conclusions

In this study, the grain boundary energy, surface energy, and work of adhesion of symmetric tilt grain boundaries in α -U have been calculated as a function of temperature and misorientation angle. Three types of STGBs (A, B, and C) are considered, which have a shear plane on either the (0 0 1), (0 1 0) or (1 0 0) planes, and corresponding tilt axes of \langle 1 0 0 \rangle , \langle 0 0 1 \rangle , and \langle 0 0 1 \rangle , respectively. Due to the orthorhombic structure of α -U, the grain boundary energy, surface energy, and work of adhesion of all three types of interface properties not only depend on the misorientation angle, but also on the interface orientation. Two of the lowest grain boundary energies are found at the ($\bar{3}$ 12 0) \langle 1 0 0 \rangle and (0 18 $\bar{2}5$) \langle 0 0 1 \rangle orientations. These two STGBs can potentially form twins, as they have a very low GB energy. It is found that the (0 9 $\bar{1}0$) \langle 0 0 1 \rangle STGB has the lowest work of adhesion, which indicates that it is the most probable site for grain boundary failure among the studied STGBs. When STGBs have a (1 0 0) shear plane, a \langle 0 0 1 \rangle tilt axis, and a (0 1 0) tilt plane (type C), they typically have a higher energy compared to the other two types (A and B) of STGBs studied. However, if the STGB has a (0 0 1) shear plane, a \langle 1 0 0 \rangle tilt axis, and a (0 1 0) tilt plane (type A), then these orientations have more resistance to failure (higher WAd). There is no consistent correlation as a function of misorientation angle for GB energy, surface energy, or WAd. At 500 K, the global arithmetic average of the surface energy (1.23 J/m²) is approximately 1.5 times the GB energy

(0.79 J/m²), and the WAd is approximately twice the GB energy (1.68 J/m²). From the current analysis it is ascertained that as the temperature increases, both the GB and surface energy tend to increase, with the GB energy increasing more rapidly, leading to a decrease in the WAd with temperature. With respect to room temperature (300 K), values at 600 K have changed by an average of 34.2% for GB energy, 5.7% for surface energy, and 10.1% for the WAd.

This study has provided the most comprehensive analysis of GBs and surfaces in α -U to date, illuminating the dependence of interfacial properties on crystallographic orientations and temperature, in addition to providing key geometrically averaged interfacial energy values. The information from this work will be utilized to study grain boundary evolution in polycrystalline α -U and deformation under irradiation, leading to the development of improved fuel performance models via physics-based mesoscale models.

5. Acknowledgement

Work supported through the INL Laboratory Directed Research and Development (LDRD) Program under DOE Idaho Operations Office Contract DE-AC07-05ID14517. This manuscript has been authored by Battelle Energy Alliance, LLC with the U.S. Department of Energy. The publisher, by accepting the article for publication, acknowledges that the U.S. Government retains a nonexclusive, paid-up, irrevocable, worldwide license to publish or reproduce the published form of this manuscript, or allow others to do so, for U.S. Government purposes. This research made use of the resources of the High-Performance Computing Center at Idaho National Laboratory, which is supported by the Office of Nuclear Energy of the U.S. Department of Energy and the Nuclear Science User Facilities [54] [55] [56].

References

- [1] W. Carmack, D. Porter, Y. Chang, S. Hayes, M. Meyer, D. Burkes, C. Lee, T. Mizuno, F. Delage, J. Somers, Metallic fuels for advanced reactors, *Journal of Nuclear Materials* 392 (2) (2009) 139 – 150, *nuclear Fuels and Structural Materials 2*. doi:<https://doi.org/10.1016/j.jnucmat.2009.03.007>. URL <http://www.sciencedirect.com/science/article/pii/S0022311509004103>
- [2] G. L. Hofman, *Metallic Fuels*, 2015, pp. 1–53. arXiv:<https://onlinelibrary.wiley.com/doi/pdf/10.1002/9783527603978.mst0105.pub2>, doi:10.1002/9783527603978.mst0105.pub2. URL <https://onlinelibrary.wiley.com/doi/abs/10.1002/9783527603978.mst0105.pub2>
- [3] G. Hofman, S. Hayes, M. Petri, Temperature gradient driving constituent redistribution in U-Zr alloys, *J. Nucl. Mater.* 227 (1996) 277.
- [4] B. Beeler, C. Deo, M. Baskes, M. Okuniewski, First principles calculations of the structure and elastic constants of α , β and γ uranium, *Journal of Nuclear Materials* 433 (1) (2013) 143 – 151. doi:<https://doi.org/10.1016/j.jnucmat.2012.09.019>. URL <http://www.sciencedirect.com/science/article/pii/S0022311512004965>

- 545 [5] N. Stojić, J. Davenport, M. Komelj, J. Glimm, Prediction of a surface magnetic moment in alpha-uranium (03 2003).
- [6] E. Y. Chen, C. Deo, R. Dingreville, Atomistic simulations of temperature and direction dependent threshold displacement energies in α - and γ -uranium, *Computational Materials Science* 157 (2019) 75 – 86. doi:<https://doi.org/10.1016/j.commatsci.2018.10.026>.
- 550 URL <http://www.sciencedirect.com/science/article/pii/S0927025618306967>
- [7] F. C. Frank, A note on twinning in alpha-uranium, *Acta Metallurgica* 1 (1953) 71 – 74.
- [8] R. W. Cahn, Twinning and slip in α uranium, *Acta Crystal* 4 (1951) 470.
- [9] L. T. Lloyd, C. S. Barrett, Thermal expansion of alpha uranium, *Journal of Nuclear Materials* 18 (1966) 55 – 59.
- 555 [10] E. S. Fisher, Temperature dependence of the elastic moduli in alpha uranium single crystals, part iv (298 k to 923 k), *Journal of Nuclear Materials* 18 (1966) 39 – 54.
- [11] B. A. Loomis, T. H. Blewitt, A. C. Klank, S. B. Gerber, Elongation of uranium single crystals during neutron irradiation, *Applied Physics Letters* 5 (7) (1964) 135–137. arXiv:<https://doi.org/10.1063/1.1754086>, doi:10.1063/1.1754086.
- 560 URL <https://doi.org/10.1063/1.1754086>
- [12] T. J. Barrett, R. J. McCabe, D. W. Brown, B. Clausen, S. C. Vogel, M. Knezevic, Predicting deformation behavior of α -uranium during tension, compression, load reversal, rolling, and sheet forming using elasto-plastic, multi-level crystal plasticity coupled with finite elements, *Journal of the Mechanics and Physics of Solids* 138 (2020) 103924. doi:<https://doi.org/10.1016/j.jmps.2020.103924>.
- 565 URL <http://www.sciencedirect.com/science/article/pii/S0022509620301605>
- [13] G. Gottstein, L. S. Shvindlerman, Grain boundary migrations in metals: thermodynamics, kinetics, applications, CRC Press, 2010.
- [14] D. A. Carpenter, J. L. Pugh, D. F. Teter, Control of grain boundaries in orthorhombic alpha-uranium, *Microscopy and Microanalysis* 11 (S02) (2005) 1792–1793. doi:10.1017/S1431927605506640.
- 570 [15] B. A. Bilby, A. G. Crocker, The theory of the crystallography of deformation twinning, *Proceedings of the Royal Society of London. Series A, Mathematical and Physical Sciences* 288 (1413) (1965) 240–255. URL <http://www.jstor.org/stable/2415026>
- [16] M. Steiner, R. McCabe, E. Garlea, S. Agnew, Monte carlo modeling of recrystallization processes in α -uranium, *Journal of Nuclear Materials* 492 (2017) 74 – 87. doi:<https://doi.org/10.1016/j.jnucmat.2017.04.026>.
- 575 URL <http://www.sciencedirect.com/science/article/pii/S0022311516310212>

- [17] M. Knezevic, R. J. McCabe, C. N. Tomé, R. A. Lebensohn, S. R. Chen, C. M. Cady, G. T. Gray III, B. Mihaila, Modeling mechanical response and texture evolution of α -uranium as a function of strain rate and temperature using polycrystal plasticity, *International Journal of Plasticity* 43 (2013) 70 – 84. doi:<https://doi.org/10.1016/j.ijplas.2012.10.011>.
URL <http://www.sciencedirect.com/science/article/pii/S0749641912001647>
- [18] R. W. Cahn, Plastic deformation of α uranium ;twinning and slip, *Acta Metallurgica* 1 (1953) 49 – 70.
- [19] R. O. Teeg, R. E. Ogilvie, Effect of orientation and temperature on the modes of deformation of uranium, *Journal of Nuclear Materials* 3, No. 1 (1961) 81 – 88.
- 585 [20] A. G. Ccocker, The crystallography of reformation thinning in alpha-uranium, *Journal of Nuclear Materials* 16 (1965) 306 – 326.
- [21] J. Rest, Kinetics of fission-gas-bubble-nucleated void swelling of the alpha-uranium phase of irradiated u-zr and u-pu-zr fuel, *Journal of Nuclear Materials* 207 (1993) 192 – 204. doi:[https://doi.org/10.1016/0022-3115\(93\)90261-V](https://doi.org/10.1016/0022-3115(93)90261-V).
590 URL <http://www.sciencedirect.com/science/article/pii/002231159390261V>
- [22] C. L. Angerman, J. G. R. Caskey, Swelling of uranium by mechanical cavitation, *Journal of Nuclear Materials* 13, No. 2 (1964) 182 – 196.
- [23] R. McCabe, A. Richards, D. Coughlin, K. Clarke, I. Beyerlein, M. Knezevic, Microstructure effects on the recrystallization of low-symmetry alpha-uranium, *Journal of Nuclear Materials* 465 (2015) 189 –
595 195. doi:<https://doi.org/10.1016/j.jnucmat.2015.04.055>.
URL <http://www.sciencedirect.com/science/article/pii/S0022311515002743>
- [24] G. S. Rohrer, Grain boundary energy anisotropy: a review, *Journal of Materials Science* 46 (2011) 5881 – 5895. doi:<https://doi.org/10.1007/s10853-011-5677-3>.
URL <https://doi.org/10.1007/s10853-011-5677-3>
- 600 [25] E. Bourasseau, A. Mouret, P. Fantou, X. Iltis, R. Belin, Experimental and simulation study of grain boundaries in UO_2 , *Journal of Nuclear Materials* 517 (02 2019). doi:[10.1016/j.jnucmat.2019.02.033](https://doi.org/10.1016/j.jnucmat.2019.02.033).
- [26] J. E. Bainbridge, B. Hijdson, On the techniques for observing fission gas bubbles in uranium, *Journal of Nuclear Materials* 17 (1965) 237 – 244.
- [27] J. Kollár, L. Vitos, H. L. Skriver, Surface energy and work function of the light actinides, *Phys. Rev. B* 49 (1994) 11288–11292. doi:[10.1103/PhysRevB.49.11288](https://doi.org/10.1103/PhysRevB.49.11288).
605 URL <https://link.aps.org/doi/10.1103/PhysRevB.49.11288>

- [28] C. D. Taylor, Evaluation of first-principles techniques for obtaining materials parameters of α -uranium and the (001) α -uranium surface, *Phys. Rev. B* 77 (2008) 094119. doi:10.1103/PhysRevB.77.094119. URL <https://link.aps.org/doi/10.1103/PhysRevB.77.094119>
- 610 [29] S.-Q. Huang, X.-H. Ju, First-principles study of properties of alpha uranium crystal and seven alpha uranium surfaces, *Journal of Chemistry* 2017 (2017). doi:<https://doi.org/10.1155/2017/8618340>.
- [30] D. Wolf, Structure-energy correlation for grain boundaries in f.c.c. metals—iii. symmetrical tilt boundaries, *Acta Metallurgica et Materialia* 38 (5) (1990) 781 – 790. doi:[https://doi.org/10.1016/0956-7151\(90\)90030-K](https://doi.org/10.1016/0956-7151(90)90030-K).
615 URL <http://www.sciencedirect.com/science/article/pii/095671519090030K>
- [31] S. Plimpton, Fast parallel algorithms for short-range molecular dynamics, *J. Comp. Phys.* 117 (1995) 1–19.
- [32] T. Frolov, W. Setyawan, R. J. Kurtz, J. Marian, A. R. Oganov, R. E. Rudd, Q. Zhu, Grain boundary phases in bcc metals, *Nanoscale* 10 (2018) 8253–8268. doi:10.1039/C8NR00271A.
620 URL <http://dx.doi.org/10.1039/C8NR00271A>
- [33] A. Stukowski, Visualization and analysis of atomis simulation data with ovito - the open visulaization tool, *Modeling and Simulation of Materials Science and Engineering* 18 (2010) 015012.
- [34] A. A. Rezwan, A. M. Jokisaari, M. R. Tonks, Modeling brittle fracture due to anisotropic thermal expansion in polycrystalline materials, *Computational Materials Science* 194 (2021) 110407. doi:<https://doi.org/10.1016/j.commatsci.2021.110407>.
625 URL <https://www.sciencedirect.com/science/article/pii/S0927025621001324>
- [35] S. Starikov, L. Kolotova, A. Kuksin, D. Smirnova, V. Tseplyaev, Atomistic simulation of cubic and tetragonal phases of u-mo alloy: Structure and thermodynamic properties, *Journal of Nuclear Materials* 499 (2018) 451 – 463. doi:<https://doi.org/10.1016/j.jnucmat.2017.11.047>.
630 URL <http://www.sciencedirect.com/science/article/pii/S0022311517312229>
- [36] B. Beeler, M. Baskes, D. Andersson, M. W. Cooper, Y. Zhang, Molecular dynamics investigation of grain boundaries and surfaces in U_3Si_2 , *Journal of Nuclear Materials* 514 (2019) 290 – 298. doi:<https://doi.org/10.1016/j.jnucmat.2018.12.008>.
URL <http://www.sciencedirect.com/science/article/pii/S0022311518312285>
- 635 [37] B. Beeler, A. Casagrande, L. Aagesen, Y. Zhang, S. Novascone, Atomistic calculations of the surface energy as a function of composition and temperature in γ U–Zr to inform fuel performance modeling, *Journal of Nuclear Materials* 540 (11 2020). doi:10.1016/j.jnucmat.2020.152271.

- [38] J. Stobo, C. Robinson, G. May, W. Blackburn, Preferred orientations in alpha uranium, *Acta Metallurgica* 13 (6) (1965) 629 – 634. doi:[https://doi.org/10.1016/0001-6160\(65\)90125-2](https://doi.org/10.1016/0001-6160(65)90125-2).
640 URL <http://www.sciencedirect.com/science/article/pii/0001616065901252>
- [39] R. Field, R. McCabe, D. Alexander, D. Teter, Deformation twinning and twinning related fracture in coarse-grained α -uranium, *Journal of Nuclear Materials* 392 (1) (2009) 105 – 113. doi:<https://doi.org/10.1016/j.jnucmat.2009.03.054>.
URL <http://www.sciencedirect.com/science/article/pii/S0022311509004735>
- 645 [40] R. McCabe, L. Capolungo, P. Marshall, C. Cady, C. Tomé, Deformation of wrought uranium: Experiments and modeling, *Acta Materialia* 58 (16) (2010) 5447 – 5459. doi:<https://doi.org/10.1016/j.actamat.2010.06.021>.
URL <http://www.sciencedirect.com/science/article/pii/S1359645410003757>
- [41] C. Calhoun, J. Wollmershauser, D. Brown, R. Mulay, E. Garlea, S. Agnew, Thermal residual strains in depleted α -U, *Scripta Materialia* 69 (8) (2013) 566 – 569. doi:<https://doi.org/10.1016/j.scriptamat.2013.06.004>.
650 URL <http://www.sciencedirect.com/science/article/pii/S1359646213003060>
- [42] R. McCabe, R. Field, D. Brown, D. Alexander, C. Cady, Electron backscatter diffraction (ebbsd) characterization of twinning related deformation and fracture in α -uranium, *Microscopy and Microanalysis* 14 (S2) (2008) 638–639. doi:[10.1017/S1431927608083554](https://doi.org/10.1017/S1431927608083554).
655 URL <https://doi.org/10.1017/S1431927608083554>
- [43] P. Zhou, D. Xiao, W. Wang, G. Sang, Y. Zhao, D. Zou, L. He, Twinning behavior of polycrystalline alpha-uranium under quasi static compression, *Journal of Nuclear Materials* 478 (2016) 83 – 90. doi:<https://doi.org/10.1016/j.jnucmat.2016.05.041>.
URL <http://www.sciencedirect.com/science/article/pii/S002231151630246X>
- 660 [44] B. Beeler, Y. Zhang, Y. Gao, An atomistic study of grain boundaries and surfaces in γ U-Mo, *Journal of Nuclear Materials* 507 (2018) 248 – 257. doi:<https://doi.org/10.1016/j.jnucmat.2018.05.007>.
URL <http://www.sciencedirect.com/science/article/pii/S0022311518301454>
- [45] Q. Zhu, A. Samanta, B. Li, R. E. Rudd, T. Frolov, Predicting phase behavior of grain boundaries with evolutionary search and machine learning, *Nature Communications* 9 (02 2018). doi:[10.1038/s41467-018-02937-2](https://doi.org/10.1038/s41467-018-02937-2).
665 URL <https://doi.org/10.1038/s41467-018-02937-2>
- [46] T. Frolov, D. L. Olmsted, M. Asta, Y. Mishin, Structural phase transformations in metallic grain boundaries, *Nature Communications* 4 (05 2013). doi:[10.1038/ncomms2919](https://doi.org/10.1038/ncomms2919).
URL <https://doi.org/10.1038/ncomms2919>

- 670 [47] P. Nikolopoulos, S. Nazaré, F. Thümmel, Surface, grain boundary and interfacial energies in UO_2
and UO_2 -Ni, *Journal of Nuclear Materials* 71 (1) (1977) 89 – 94. doi:[https://doi.org/10.1016/
0022-3115\(77\)90191-X](https://doi.org/10.1016/0022-3115(77)90191-X).
URL <http://www.sciencedirect.com/science/article/pii/002231157790191X>
- [48] D. Brown, M. Bourke, B. Clausen, D. Korzekwa, R. Korzekwa, R. McCabe, T. Sisneros, D. Teter,
675 Temperature and direction dependence of internal strain and texture evolution during deformation of
uranium, *Materials Science and Engineering: A* 512 (1) (2009) 67 – 75. doi:[https://doi.org/10.
1016/j.msea.2009.02.004](https://doi.org/10.1016/j.msea.2009.02.004).
URL <http://www.sciencedirect.com/science/article/pii/S0921509309001452>
- [49] D. M. R. Taplin, J. W. Martin, The effect of grain size and cold work on the tensile properties of
680 alpha-uranium, *Journal of the Less- common Metals* 7 (1964) 89 – 97.
- [50] C. D. Taylor, Erratum: Evaluation of first-principles techniques for obtaining materials parameters of
alpha-uranium and the (001) alpha-uranium surface [*phys. rev. b* 77, 094119 (2008)], *Phys. Rev. B* 80 (2009)
149906. doi:10.1103/PhysRevB.80.149906.
URL <https://link.aps.org/doi/10.1103/PhysRevB.80.149906>
- 685 [51] N. R. Williams, M. Molinari, S. C. Parker, M. T. Storr, Atomistic investigation of the structure and
transport properties of tilt grain boundaries of UO_2 , *Journal of Nuclear Materials* 458 (2015) 45–55.
doi:<https://doi.org/10.1016/j.jnucmat.2014.11.120>.
URL <https://www.sciencedirect.com/science/article/pii/S0022311514009271>
- [52] T. K. B. R. D. Leggett, B. Mastel, Irradiation behaviour of high purity uranium, Hanford Laboratories,
690 HW- 79559 (November 1963).
- [53] A. Jokisaari, Irradiation-induced internal stresses in polycrystalline alpha-uranium: a mesoscale mechanical
approach, *Computational Materials Science* 176 (2020) 109545. doi:[https://doi.org/10.1016/j.
commatsci.2020.109545](https://doi.org/10.1016/j.commatsci.2020.109545).
URL <http://www.sciencedirect.com/science/article/pii/S0927025620300367>
- 695 [54] K. Mahbuba, B. Beeler, A. Jokisaari, Evaluation of the anisotropic grain boundaries and surfaces of -u
via molecular dynamics, *Journal of Nuclear Materials* 554 (2021) 153072. doi:[https://doi.org/10.
1016/j.jnucmat.2021.153072](https://doi.org/10.1016/j.jnucmat.2021.153072).
URL <https://www.sciencedirect.com/science/article/pii/S0022311521002956>
- [55] M. Cooper, K. Gamble, L. Capolungo, C. Matthews, D. Andersson, B. Beeler, C. Stanek, K. Metzger,
700 Irradiation-enhanced diffusion and diffusion-limited creep in U_3Si_2 , *Journal of Nuclear Materials* 555
(2021) 153129. doi:<https://doi.org/10.1016/j.jnucmat.2021.153129>.
URL <https://www.sciencedirect.com/science/article/pii/S0022311521003524>

[56] Y. Mishin, C. Herzig, Diffusion in the ti-al system, Acta Materialia 48 (3) (2000) 589–623. doi:[https://doi.org/10.1016/S1359-6454\(99\)00400-0](https://doi.org/10.1016/S1359-6454(99)00400-0).

705

URL <https://www.sciencedirect.com/science/article/pii/S1359645499004000>

6. Appendix

Table 1: Studied STGBs of α -U.

type A		type B		type C	
tilting axis	$\langle 1\ 0\ 0 \rangle$	tilting axis	$\langle 0\ 0\ 1 \rangle$	tilting axis	$\langle 0\ 0\ 1 \rangle$
tilt plane or cut plane	$(0\ 1\ 0)$	tilt plane or cut plane	$(1\ 0\ 0)$	tilt plane or cut plane	$(0\ 1\ 0)$
shear plane	$(0\ 0\ 1)$	shear plane	$(0\ 1\ 0)$	shear plane	$(1\ 0\ 0)$
misorientation angle (deg)	STGB plane	misorientation angle (deg)	STGB plane	misorientation angle (deg)	STGB plane
9.53	$(\bar{6}\ 1\ 0)$	5.72	$(\bar{3}\ 0\ 100)$	5.72	$(0\ 3\ \bar{5}0)$
14.25	$(\bar{1}2\ 3\ 0)$	12.68	$(\bar{1}\ 0\ 15)$	11.42	$(0\ 3\ \bar{2}5)$
18.93	$(\bar{3}\ 1\ 0)$	18.92	$(\bar{1}\ 0\ 10)$	22.62	$(0\ 6\ \bar{2}5)$
28.07	$(\bar{6}\ 3\ 0)$	22.62	$(\bar{3}\ 0\ 25)$	33.4	$(0\ 9\ \bar{2}5)$
36.87	$(\bar{3}\ 2\ 0)$	36.87	$(\bar{1}\ 0\ 5)$	57.22	$(0\ 36\ \bar{5}5)$
53.13	$(\bar{3}\ 3\ 0)$	45.24	$(\bar{1}\ 0\ 4)$	61.93	$(0\ 18\ \bar{2}5)$
90	$(\bar{3}\ 6\ 0)$	61.93	$(\bar{9}\ 0\ 25)$	67.38	$(0\ 4\ \bar{5})$
126.87	$(\bar{3}\ 12\ 0)$	79.61	$(\bar{1}\ 0\ 2)$	73.74	$(0\ 9\ \bar{1}0)$
136.4	$(\bar{3}\ 15\ 0)$	90	$(\bar{3}\ 0\ 5)$	90	$(0\ 6\ \bar{5})$
143.13	$(\bar{1}\ 6\ 0)$	126.87	$(\bar{6}\ 0\ 5)$	100.39	$(0\ 36\ \bar{2}5)$
151.93	$(\bar{3}\ 24\ 0)$	146.6	$(\bar{2}\ 0\ 1)$	112.62	$(0\ 9\ \bar{5})$
161.08	$(\bar{1}\ 12\ 0)$	161.08	$(\bar{1}8\ 0\ 5)$	126.87	$(0\ 12\ \bar{5})$
198.93	$(\bar{1}\ \bar{1}2\ 0)$	198.93	$(\bar{1}8\ 0\ \bar{5})$	134.76	$(0\ 72\ \bar{2}5)$
208.07	$(\bar{3}\ \bar{2}4\ 0)$	213.4	$(\bar{2}\ 0\ \bar{1})$	143.13	$(0\ 18\ \bar{5})$
216.87	$(\bar{1}\ \bar{6}\ 0)$	233.13	$(\bar{6}\ 0\ \bar{5})$	161.08	$(0\ 36\ \bar{5})$
223.6	$(\bar{3}\ \bar{1}5\ 0)$	270	$(\bar{3}\ 0\ \bar{5})$	170.47	$(0\ 72\ \bar{5})$
233.13	$(\bar{3}\ \bar{1}2\ 0)$	280.39	$(\bar{1}\ 0\ \bar{2})$	189.53	$(0\ 72\ \bar{5})$
270	$(\bar{3}\ \bar{6}\ 0)$	298.07	$(\bar{9}\ 0\ \bar{2}5)$	198.93	$(0\ 36\ \bar{5})$
306.87	$(\bar{3}\ \bar{3}\ 0)$	314.76	$(\bar{1}\ 0\ \bar{4})$	216.87	$(0\ 18\ \bar{5})$
323.13	$(\bar{3}\ \bar{2}\ 0)$	323.13	$(\bar{1}\ 0\ \bar{5})$	225.24	$(0\ 72\ \bar{2}5)$
331.93	$(\bar{6}\ \bar{3}\ 0)$	337.38	$(\bar{3}\ 0\ \bar{2}5)$	233.13	$(0\ 12\ \bar{5})$
341.08	$(\bar{3}\ \bar{1}\ 0)$	341.08	$(\bar{1}\ 0\ \bar{1}0)$	247.38	$(0\ 9\ \bar{5})$
345.75	$(\bar{1}2\ \bar{3}\ 0)$	347.32	$(\bar{1}\ 0\ \bar{1}5)$	259.61	$(0\ 36\ \bar{2}5)$
350.47	$(\bar{6}\ \bar{1}\ 0)$	354.28	$(\bar{3}\ 0\ \bar{1}00)$	270	$(0\ 6\ \bar{5})$
				286.26	$(0\ 9\ \bar{1}0)$
				292.26	$(0\ 4\ \bar{5})$
				298.08	$(0\ \bar{1}8\ \bar{2}5)$
				302.78	$(0\ 36\ \bar{5}5)$
				326.61	$(0\ 9\ \bar{2}5)$
				337.38	$(0\ 6\ \bar{2}5)$
				348.58	$(0\ 3\ \bar{2}5)$
				354.28	$(0\ 3\ \bar{5}0)$

Table 2: Studied surfaces related to STGBs of α -U.

type A		type B		type C	
tilting axis	$\langle 1\ 0\ 0 \rangle$	tilting axis	$\langle 0\ 0\ 1 \rangle$	tilting axis	$\langle 0\ 0\ 1 \rangle$
tilt plane or cut plane	$(0\ 1\ 0)$	tilt plane or cut plane	$(1\ 0\ 0)$	tilt plane or cut plane	$(0\ 1\ 0)$
shear plane	$(0\ 0\ 1)$	shear plane	$(0\ 1\ 0)$	shear plane	$(1\ 0\ 0)$
misorientation angle (deg)	STGB plane	misorientation angle (deg)	STGB plane	misorientation angle (deg)	STGB plane
4.765	$(\bar{6}\ 1\ 0)$	2.86	$(\bar{3}\ 0\ 100)$	2.86	$(0\ 3\ \bar{5}0)$
7.125	$(\bar{1}2\ 3\ 0)$	6.34	$(\bar{1}\ 0\ 15)$	5.71	$(0\ 3\ \bar{2}5)$
9.465	$(\bar{3}\ 1\ 0)$	9.46	$(\bar{1}\ 0\ 10)$	11.31	$(0\ 6\ \bar{2}5)$
14.035	$(\bar{6}\ 3\ 0)$	11.31	$(\bar{3}\ 0\ 25)$	16.7	$(0\ 9\ \bar{2}5)$
18.435	$(\bar{3}\ 2\ 0)$	18.435	$(\bar{1}\ 0\ 5)$	28.61	$(0\ 36\ \bar{5}5)$
26.565	$(\bar{3}\ 3\ 0)$	22.62	$(\bar{1}\ 0\ 4)$	30.965	$(0\ 18\ \bar{2}5)$
45	$(\bar{3}\ 6\ 0)$	30.965	$(\bar{9}\ 0\ 25)$	33.69	$(0\ 4\ \bar{5})$
63.435	$(\bar{3}\ 12\ 0)$	39.805	$(\bar{1}\ 0\ 2)$	36.87	$(0\ 9\ \bar{1}0)$
68.2	$(\bar{3}\ 15\ 0)$	45	$(\bar{3}\ 0\ 5)$	45	$(0\ 6\ \bar{5})$
71.565	$(\bar{1}\ 6\ 0)$	63.435	$(\bar{6}\ 0\ 5)$	50.195	$(0\ 36\ \bar{2}5)$
75.965	$(\bar{3}\ 24\ 0)$	73.3	$(\bar{2}\ 0\ 1)$	56.31	$(0\ 9\ \bar{5})$
80.54	$(\bar{1}\ 12\ 0)$	80.54	$(\bar{1}8\ 0\ 5)$	63.435	$(0\ 12\ \bar{5})$
99.465	$(\bar{1}\ \bar{1}2\ 0)$	99.465	$(\bar{1}8\ 0\ \bar{5})$	67.38	$(0\ 72\ \bar{2}5)$
104.035	$(\bar{3}\ \bar{2}4\ 0)$	106.7	$(\bar{2}\ 0\ \bar{1})$	71.565	$(0\ 18\ \bar{5})$
108.435	$(\bar{1}\ \bar{6}\ 0)$	116.565	$(\bar{6}\ 0\ \bar{5})$	80.54	$(0\ 36\ \bar{5})$
111.8	$(\bar{3}\ \bar{1}5\ 0)$	135	$(\bar{3}\ 0\ \bar{5})$	85.235	$(0\ 72\ \bar{5})$
116.565	$(\bar{3}\ \bar{1}2\ 0)$	140.195	$(\bar{1}\ 0\ \bar{2})$	94.765	$(0\ \bar{7}2\ \bar{5})$
135	$(\bar{3}\ \bar{6}\ 0)$	149.035	$(\bar{9}\ 0\ \bar{2}5)$	99.465	$(0\ 36\ \bar{5})$
153.435	$(\bar{3}\ \bar{3}\ 0)$	157.38	$(\bar{1}\ 0\ \bar{4})$	108.435	$(0\ 18\ \bar{5})$
161.565	$(\bar{3}\ \bar{2}\ 0)$	161.565	$(\bar{1}\ 0\ \bar{5})$	112.62	$(0\ \bar{7}2\ \bar{2}5)$
165.965	$(\bar{6}\ \bar{3}\ 0)$	168.69	$(\bar{3}\ 0\ \bar{2}5)$	116.565	$(0\ 12\ \bar{5})$
170.54	$(\bar{3}\ \bar{1}\ 0)$	170.54	$(\bar{1}\ 0\ \bar{1}0)$	123.69	$(0\ \bar{9}\ \bar{5})$
172.875	$(\bar{1}2\ \bar{3}\ 0)$	173.66	$(\bar{1}\ 0\ \bar{1}5)$	129.805	$(0\ \bar{3}6\ \bar{2}5)$
175.235	$(\bar{6}\ \bar{1}\ 0)$	177.14	$(\bar{3}\ 0\ \bar{1}00)$	135	$(0\ \bar{6}\ \bar{5})$
				143.13	$(0\ \bar{9}\ \bar{1}0)$
				146.13	$(0\ \bar{4}\ \bar{5})$
				149.04	$(0\ \bar{1}8\ \bar{2}5)$
				151.39	$(0\ \bar{3}6\ \bar{5}5)$
				163.305	$(0\ \bar{9}\ \bar{2}5)$
				168.69	$(0\ \bar{6}\ \bar{2}5)$
				174.29	$(0\ \bar{3}\ \bar{2}5)$
				177.14	$(0\ \bar{3}\ \bar{5}0)$

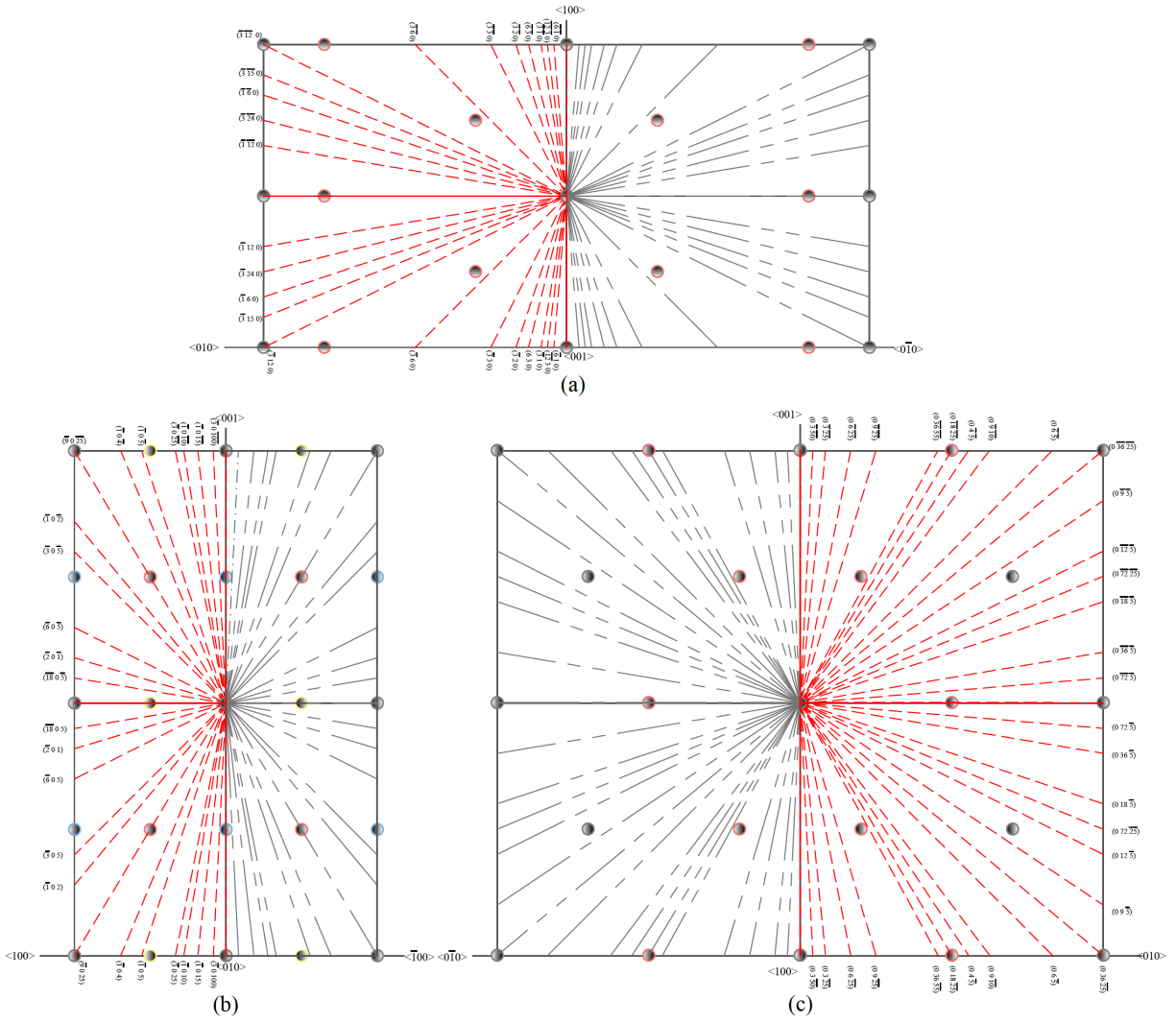


Figure 10: Schematic diagram of symmetric tilt grain boundaries (STGB) of (a) type A, (b) type B, and (c) type C along with the supercell axis. In each diagram four unit cells are shown, with gray colored planes (large dash) the mirror image of red-colored planes (small dash) of the α -U lattice. To illustrate the misorientation angles in a sequential manner, here the authors have shifted the planes (keeping their tilt angle with tilting plane same) to the same lattice point.